Mon. Not. R. Astron. Soc. **000**, 000–000 () Printed 4 November 2015 (MN LATEX style file v2.2)

Large and small-scale structure of the Intermediate and High Velocity Clouds towards the LMC and SMC

J. V. Smoker[1⋆], A. J. Fox[2], F. P. Keenan[3]
[1] *European Southern Observatory, Alonso de Cordova 3107, Casilla 19001, Vitacura, Santiago 19, Chile*
[2] *Space Telescope Science Institute, 3700 San Martin Drive, Baltimore MD 21218, USA*
[3] *Astrophysics Research Centre, School of Mathematics and Physics, Queen's University Belfast, Belfast, BT7 1NN*

arXiv:1511.00843v1 [astro-ph.GA] 3 Nov 2015

Accepted Received in original form

ABSTRACT

We employ Ca II K and Na I D interstellar absorption-line spectroscopy of early-type stars in the Large and Small Magellanic Clouds to investigate the large- and small-scale structure in foreground Intermediate and High Velocity Clouds (I/HVCs). These data include FLAMES-GIRAFFE Ca II K observations of 403 stars in four open clusters, plus FEROS or UVES spectra of 156 stars in the LMC and SMC. The FLAMES observations are amongst the most extensive probes to date of Ca II structures on ∼20 arcsec scales in Magellanic I/HVCs.

From the FLAMES data within a 0.5° field-of-view, the Ca II K equivalent width in the I/HVC components towards three clusters varies by factors of ≥10. There are no detections of molecular gas in absorption at intermediate or high velocities, although molecular absorption is present at LMC and Galactic velocities towards some sightlines. The sightlines show variations in EW exceeding a factor ∼7 in CH^+ towards NGC 1761 over scales of less than 10 arcminutes.

The FEROS/UVES data show Ca II K I/HVC absorption in ∼60 per cent of sightlines. No Na I D is found at non-Magellanic HVC velocities aside from a tentative detection towards the star LHA 120-S 93. The range in the Ca II/Na I ratio in I/HVCs is from –0.45 to +1.5 dex, similar to previous measurements for I/HVCs. In ten sightlines we find Ca II/O I ratios in I/HVC gas ranging from 0.2 to 1.5 dex below the solar value, indicating either dust or ionisation effects. In nine sightlines I/HVC gas is detected in both H I and Ca II, and shows similar Ca II/H I ratios to typical I/HVCs, and similar velocities, implying that in these sightlines the two elements form part of the same structure.

Key words: ISM: general – ISM: clouds – ISM: abundances – ISM: structure – Galaxies: Magellanic Clouds – Open clusters and associations: Individual: NGC 330, NGC 346, NGC 1761, NGC 2004

1 INTRODUCTION

High velocity clouds (HVCs) were discovered over 50 years ago (Muller, Oort & Raimond 1963). Originally observed in H I, they consist of parcels of gas with velocities not compatible with Galactic rotation; in practice this means HVCs have $|v_{\rm LSR}|$ >90–100 km s^{-1} if they lie at at high Galactic latitudes. Clouds with ∼40 < $|v_{\rm LSR}|$ < 90 km s^{-1} are referred to as Intermediate Velocity Clouds (IVCs). Recently it has become clear that at least some of the clouds lie within the halo of the Milky Way; for example Complex A (van Woerden et al. 1999), Complex WB (Thom et al. 2006), Complex C (Wakker et al. 2007, Thom et al. 2008), as well as the Cohen Stream, Complex GCP, and Complex g1 (Wakker et al. 2008).

Although some HVCs may be large clouds outside of the Milky Way halo (Blitz et al. 1999), the failure to detect HVCs far from their host galaxies (Pisano et al. 2004; Westmeier, Brüns & Kerp 2008) and the lack of stars in many HVCs (e.g. Simon & Blitz 2002; Siegel et al. 2005; Hopp, Schulte-Ladbeck & Kerp 2007) argues against this hypoth-

⋆ email: jsmoker@eso.org Based on ESO programme IDs 078.C-0493(A) and 171.D-0237(B).

ysis. Likewise, comparison of the probability of detection of ionised HVCs in AGN and Galactic halo stellar sightlines by Lehner & Howk (2011) indicate that HVCs at velocities between ∼90 and 170 km s^{-1} likely reside within the halo of the Milky Way and are not further away structures within the local group. These clouds may have formed by the accretion of primordial gas, interaction of the Milky Way with its neighbouring galaxies via ram pressure and tidal stripping, or the Galactic Fountain (see Bregman 2004 for a review). Finally, Lehner & Howk show that HVCs at extreme velocities (>170 km s^{-1}) lie beyond the Galactic Halo and are not discussed further here.

I/HVCs are important to study as they *may* provide fuel for star formation in the Milky Way (see the review by Wakker & van Woerden 1997; Fox et al. 2014), and provide information on close encounters and/or winds from the SMC and LMC (Olano 2008; Lehner, Staveley-Smith & Howk 2009).

In the present paper we employ FLAMES Ca II K archive spectra of four open clusters in the Large and Small Magellanic Clouds (LMC, SMC) to investigate the small-scale (∼11 arcseconds to ∼25 arcminutes) structure of the I/HVCs in the lines-of-sight to these galaxies. We also use FEROS and UVES observations of 156 LMC and SMC stellar targets in Ca II K and Na I D to probe large- (degree-) scale variations in I/HVC column density. Observations of interstellar Ca and Na towards the Magellanic Clouds was first performed by Blades (1980), with subsequent observations in different wavelength bands and theoretical work by Savage & de Boer (1981), Songaila (1981), Songaila, Cowie & York (1981), Songaila et al. (1986), Andreani & Vidal-Madjar (1988), Blades et al. (1988a,b), Wayte (1990), Molaro et al. (1993), Welty et al. (1997, 1999), Richter et al. (1999), Bluhm et al. (2001), Staveley-Smith et al. (2003), André et al. (2004), Olano (2008), Lehner et al. (2009) and Welty, Xue and Wong (2012). These and other references indicate that some I/HVCs contain molecular gas and dust, often show multi-component velocity structure, and have abundance patterns sometimes consistent with those of the Magellanic Clouds and sometimes with the Milky Way. The velocity fields of Magellanic HVCs have been interpreted as being caused by spiral structure in the LMC (Blades 1980), winds from the LMC (Olano et al. 2004), or interaction of LMC/SMC and Milky Way gas (Olano et al. 2008). Background sources in the Magellanic Clouds have also been used to study the absorption-line structure within the Milky Way (e.g. André et al. 2004, Nasoudi-Shoar et al. 2010, van Loon et al. 2013; Smoker, Keenan & Fox 2015).

Our paper is laid out as follows. Section 2 describes the sample of stars towards the Magellanic Clouds and a description of the data reduction for the optical spectra. In Sect. 3 we provide the main results, including the FLAMES, FEROS and UVES spectra towards the Magellanic system. Section 4 presents the discussion which covers the velocity dependence on RA of LMC I/HVCs, abundance ratios using optical and previous UV data, and large- and small-scale structure variations in Ca II K of the I/HVCs towards the LMC and SMC. Finally, Sect. 5 gives a summary of the main findings.

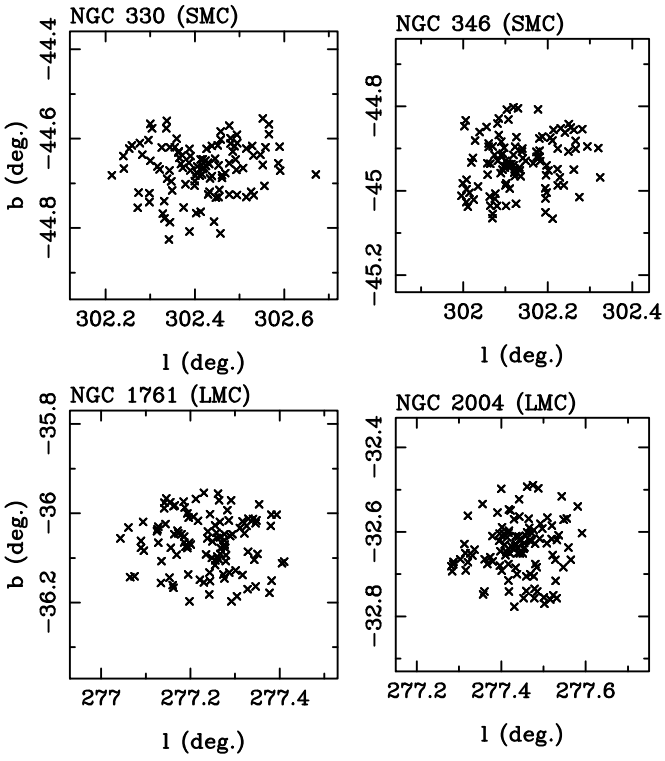

Figure 1. Location of LMC and SMC stars observed with FLAMES-GIRAFFE.

2 THE SAMPLE, OBSERVATIONS AND DATA REDUCTION

2.1 Archival FLAMES and FEROS data towards the LMC and SMC

FLAMES[1] observations towards four open clusters in the LMC and SMC were retrieved from the ESO archive and are used to study the I/HVCs towards these galaxies and their variation on small scales. Table 1 presents the basic cluster data, and Fig. 1 shows the locations of the stellar sightlines.

The FLAMES spectra use the HR2 setting, providing a spectral resolution of ∼16 km s^{-1} and wavelength coverage from ∼3850Å to 4045Å, covering the Ca II K line. Full details of the sample, data reduction and analysis are given in Smoker et al. (2015) where the structure of the low-velocity (Galactic) gas and its variation on small scales is investigated and all the spectra are presented. The S/N ratios of the spectra are ∼30 or 60 per pixel for the two SMC clusters, and 95 or 135 for the two LMC clusters. Minimum and maximum star-star separations are 11 arcsec to 27 arcmin, 14 arcsec to 20.7 arcmin, 14 arcsec to 22.2 arcmin, and 11 arcsec to 20 arcmin, respectively, for NGC 330, NGC 346, NGC 1761 and NGC 2004. These correspond to transverse separations of ∼3–500 pc at the distance of the Magellanic clouds.

[1] FLAMES (Pasquini et al. 2002) is a multi-object, intermediate and high resolution spectrograph, mounted on the VLT/Unit Telescope 2 (Kueyen) at Cerro Paranal, Chile, operated by ESO.

Table 1. Basic data for the open clusters observed with FLAMES sorted in increasing NGC number. The distances to the LMC and SMC were taken from Keller & Wood (2006). The "Scales probed" column corresponds to the minimum and maximum transverse star-star separation at the distance of the cluster.

Cluster	Alternative name	Location	(l, b) (deg.)	Dist (kpc)	Exp time (s)	Median S/N at Ca II K	Stars used	Scales probed ($'$)	Mag. scales probed (pc)
NGC 330	Kron 35	SMC	302.42, –44.66	61	13650	30	110	0.2 – 27.4	3.6 – 486
NGC 346	Kron 39	SMC	302.14, –44.94	61	6825	60	109	0.3 – 20.7	5.3 – 367
NGC 1761	LH 09	LMC	277.23, –36.07	51	13650	135	109	0.2 – 22.3	3.0 – 331
NGC 2004	KMHK 991	LMC	277.45, –32.63	51	13650	95	75	0.2 – 20.0	3.0 – 297

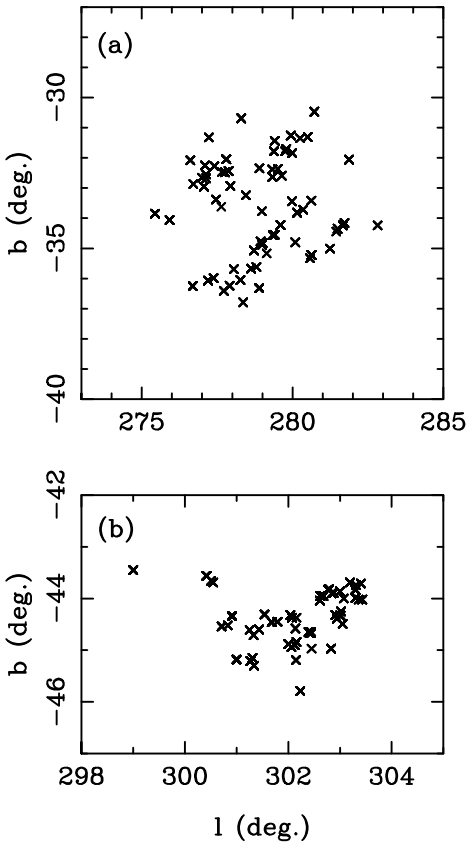

Figure 2. Location of (a) LMC and (b) SMC stars observed with FEROS and UVES.

Additionally, FEROS[2] and UVES observations towards 71 early-type stars in the LMC and 85 from the SMC were downloaded from the ESO archive. These observations have a spectral resolution of 6.3 km s^{-1} with a median S/N ratio of 35 per pixel in Ca II and 75 in Na I D. The stars observed are listed in Smoker et al. (2015), with Fig. 2 showing the location of the stars in (l, b) coordinates. The species considered in this paper are shown in Table 2.

The data were reduced using the FEROS pipeline (in MIDAS) or the reduced spectra downloaded from the ESO archive in the case of UVES. For FEROS the reduction was undertaken using both standard and optimum extraction, with and without cosmic ray removal, respectively. Agreement was found to be good between the two methods. To check the quality of the results, the equivalent widths and velocities of a handful of lines were compared with previous UVES[3] observations of a few B-type stars taken from the online version of the Paranal Observatory Project (POP) survey (Bagnulo et al. 2003). Agreement was found to be within 1 km s^{-1} for velocities and within 5 per cent for equivalent widths for strong lines.

Table 2. Main transitions studied in this paper. Wavelengths and oscillator strengths are from Morton (2003, 2004). Column 4 gives the ionisation potential (IP) in eV. For comparison the ionisation potential of H I is 13.60 eV.

Trans.	$\lambda_{\rm air}$ (Å)	f-value	IP (eV)
Ca II K	3933.661	0.627	11.87
Na I D1	5889.951	0.641	5.14
Na I D2	5895.924	0.320	5.14

The individual FEROS or UVES spectra were co-added using SCOMBINE within IRAF[4], converted into ASCII format and then read into the spectral analysis software DIPSO for further analysis. Initially this included shifting to the Kinematical Local Standard of Rest (LSR) using corrections generated by the program RV (Wallace & Clayton 1996), then normalising the spectra by fitting polynomials to the stellar continuum in the region of interest. The RMS of the normalisation procedure gives the S/N ratio in the final spectra. For the region around Na I D, telluric spectra were removed as described in Hunter et al. (2006).

Equivalent widths, velocity centroids and full width half maximum (FWHM) velocity values of the optical transitions were obtained by fitting Gaussians to the normalised spectra using the ELF package within DIPSO (Howarth et al. 2003). These results were used as initial inputs to the VAPID code (Howarth et al. 2002) which provide the final values of the column densities and b-values by curve-of-growth analysis. Errors were derived as described in Hunter et al. (2006).

[2] FEROS (Kaufer et al. 1999) is a high-resolution echelle spectrograph, mounted on the 2.2 m Telescope at La Silla, Chile, operated by ESO.

[3] UVES (Dekker et al. 2000) is a high resolution echelle spectrograph, mounted on the VLT/Unit Telescope 2 (Kueyen) at Cerro Paranal, Chile, operated by ESO.

[4] IRAF is distributed by the National Optical Astronomy Observatories, U.S.A.

2.1.1 21 cm data from the GASS and LAB surveys

For the H I 21 cm spectra, we adopt measurements from the Parkes Galactic All-Sky Survey (GASS) and LABS survey (Kalberla et al. 2005; McClure-Griffiths et al. 2009). Both surveys have spectral resolutions of $\sim$1 km s^{-1}, with spatial resolutions of $\sim$0.5° and and 16 arcmin, respectively. The vast majority of these spectra show no I/HVC detection, hence an H I map is not shown. We note that H I in I/HVCs is clumpy, with structures visible in H I emission down to the observational limit of $\sim$1 arcmin in objects such as Complex C (Smoker et al. 2001), compact HVCs (de Heij, Braun & Burton 2002), and miscellaneous IVCs (Ben Bekhti et al. 2009), and additionally in absorption down to scales of arcseconds or less for low-velocity gas (Diamond et al. 1989). Similarly, comparison of LMC hydrogen column densities derived from 21-cm H I observations compared with Lyα show variations of a factor of 2–3 in some sightlines, indicating small-scale H I structure (Welty et al. 2012). Hence there are large systematic uncertainties in the derived H I to optical line ratios derived in the current work (see Wakker 2001 for a discussion).

3 RESULTS

3.1 FLAMES-GIRAFFE Magellanic Cloud spectra in Ca II

Figures A1 to A5 (available online) show, for each cluster, the spectra of the 16 star-to-star pairs with the maximum difference in equivalent width of the intermediate- or high-velocity component, to show the variation in Ca II K I/HVC absorption-line strength. Figure 3 shows the corresponding plots for two or three objects with the strongest and weakest I/HVC component per cluster observed in Ca II K with FLAMES. All of the spectra are shown in Smoker et al. (2015), in which the low-velocity component only is discussed and where tables of the equivalent width measurements at all velocities are given.

3.2 FEROS and UVES Magellanic Cloud spectra in Ca II/Na I

Smoker et al. (2015) present FEROS and UVES Ca II K and Na I D1 spectra and Voigt profile fits of stars towards the Magellanic Clouds used in our analysis as well as the nearest GASS and LAB Survey H I 21 cm spectra.

4 DISCUSSION

4.1 Large-scale structure of I/HVCs toward the LMC

In this section we use the FEROS and UVES results to discuss the velocity field towards the LMC IVCs, component structure observed in Ca II, variation with Ca II column density with position, and finally elemental abundances using the current optical observations and previous UV data taken from Lehner et al. (2009).

4.1.1 Velocity dependence on RA for LMC I/HVCs

Due to its higher radial velocity, discriminating between HVC and Magellanic velocity components is easier for the LMC than for the SMC. Spectra for a total of 73 LMC stars exist in either Ca II or Na I D, and HV components are present in many of them. In the LMC spectra there are I/HVC components present in Ca II K at a range of velocities from $\sim$+40 km s^{-1} up to the LMC velocity of $\sim$+280 km s^{-1}. Lehner et al. (2009) find that the velocity of the HV components in the LMC standard of rest (LMCSR) correlates with Right Ascension, which they ascribe to the clouds being formed by an energetic outflow from the LMC. On the other hand, Richter et al. (2014) also find UV absorption-line profiles at high velocities some degrees away from the LMC, which is inconsitent with the outflow scenario and implies a separate origin.

The idea that some HVCs are in some way connected to the Magellanic system is not new (Giovanelli 1981; Mirabel 1981; Olano 2004 amongst others), although what fraction of them and the exact formation mechanism is still unclear (Nidever et al. 2008). Following Lehner et al., Fig. 4 shows the velocity, plotted against their RA, of all detected components in Ca II K from –50 to –200 km s^{-1} in the LMCSR, which is defined as:

$$v_{\rm LMCSR} = v_{\rm GSR} + (86 \times \cos l \cos b) + (268 \times \sin l \cos b) - (252 \times \sin b), \quad (1)$$

where $v_{\rm GSR} = v_{\rm LSR} + v_{\odot} \sin l \cos b$ is the velocity in the Galactic standard of rest frame, and $v_{\odot}$ is the solar circular rotation velocity around the Galactic centre. The solid line is the best-fit relationship of Lehner et al. (2009), and the current observations generally are offset by about +20 km s^{-1} from this. The scatter in the two datasets is similar. At RA=$\sim$05$^{\rm h}$30$^{\rm m}$ the range in v(LMCSR) is from $\sim$–100 to –170 km s^{-1}, rising to $\sim$–40 to –130 km s^{-1} at RA$\sim$5$^{\rm h}$. A few stars (SK-66 5 and SK-70 78 marked in Fig. 4) at RA$\sim$5$^{\rm h}$ show absorption features in their spectra that would be expected at higher values of RA. Figure 5 shows spectra that have LMC LSR velocities of less than –130 km s^{-1}. The features here are often close to the noise level.

4.1.2 Velocity component structure in Ca II for LMC I/HVCs from FEROS observations

I/HVC component structure is observed in some sightlines. For the IVCs these include SK-67 206, SK-67 173, SK-68 111, LHA 120-S 116 and SK-70 120, while for the HVCs include SK-67 199 (although at low S/N), SK-68 111, SK-69 43 and AzV 490 (although there is possible stellar contamination). In only one case are there corresponding UV data from Lehner et al. (2009), specifically towards SK-68 111 where these authors only find a single component with velocities of +109.6±3.8 km s^{-1} (O I), +102.4±1.4 km s^{-1} (Fe II) and +114.5±3.8 km s^{-1} (H I), compared with our Ca II K velocities for HVC components of +96.1±1.1 and +114.6±1.2 km s^{-1}. The velocity resolution for the UV data is either 7 km s^{-1} (STIS) or $\sim$20 km s^{-1} (FUSE) and with typical S/N ratios of $\sim$5–40 in the FUSE spectra, with the velocity resolution in the Parkes data being 1.6 km s^{-1} although with a much larger beam than the optical observations. In any case, we note that no component structure is listed in Table 1 of Lehner et al. (2009) in either the UV or H I data. However,

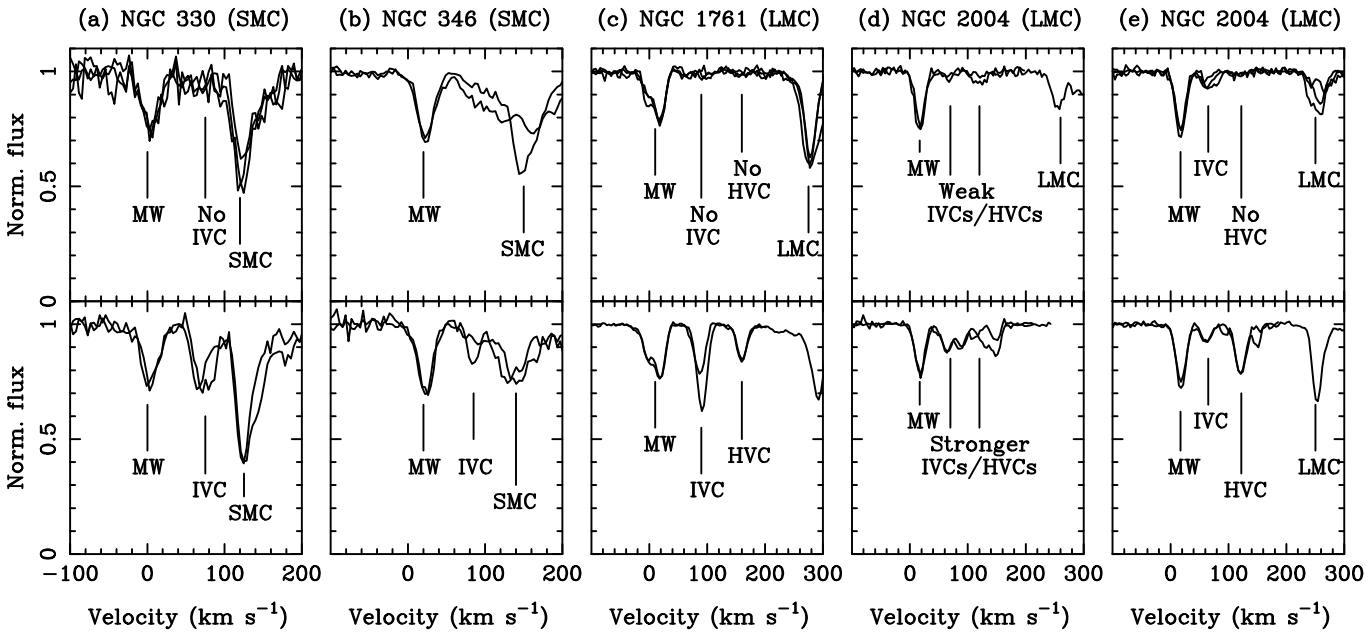

Figure 3. Ca II K spectra towards the four Magellanic clusters studied, showing two or three sightlines with the minimum (top panels) and maximum (bottom panels) equivalent width in the I/HVC components. The maximum star-to-star separation on the sky is 27 arcminutes (the size of the FLAMES plate). It is apparent that the variation in the strength of the low-velocity Ca II component is smaller than the variation in the I/HVC and Magellanic components.

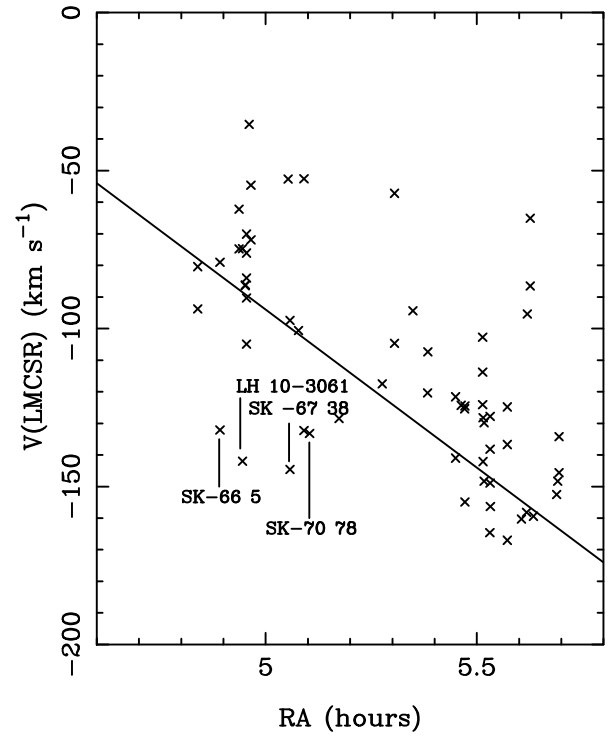

Figure 4. Velocity of high velocity components in the LMC standard of rest plotted against their RA. The solid line is the best-fit relationship of Lehner et al. (2009). Only components with LSR velocities in the range +90–175 km s^{-1} are shown.

an inspection of Fig. 1 of Lehner et al. (2009) indicates that at least for some sightlines such structure may be difficult to determine due to low S/N ratios.

Multi-component velocity profiles have been detected in other I/HVCs observed in absorption, including the Magellanic Bridge (Misawa et al. 2009), the Magellanic Stream (Fox et al. 2005, 2010), the M 15 IVC (Meyer & Lauroesch 1999; Welsh, Wheatley & Lallement 2009) and SN 1987A in the LMC (Adreani & Vidal-Madjar 1988; Blades et al 1988a,b; Welty et al. 1999). This component structure indicates that several physical regions of absorbing gas exist along the line-of-sight, and suggests but does not prove the fragmentation of initially-larger clouds. Fragmentation is also observed in deep 21 cm images of the tip of the Magellanic Stream (Stanimirović et al. 2008), and is predicted by hydrodynamic simulations of HVCs streaming through a hot corona (e.g. Bland-Hawthorn 2009). Such fragmentation may be the precursor to eventual evaporation of the I/HVCs before they reach the disk of the Milky Way (e.g. Heitsch & Putman 2009; Fox et al. 2010). A mix of fragmentation, cooling and mixing with other gas may change the ionisation structure of I/HVCs and their metalicities (Gritton et al. 2014), with non-equilibrium chemistry in diffuse interstellar gas increasing cooling (Richings, Schaye & Oppenheimer 2010) and perhaps explain the detection of Na I in some I/HVCs. If I/HVCs *do* evaporate before reaching the disk, then they must re-condense if they are to form the fuel needed to sustain star formation in the disk and to reproduce stellar abundance patterns (Kennicutt 1998, Chiappini 2008).

Finally, in eight of nine sightlines where we have measured the velocity of the *main* HVC component in Ca II and H I, the values for both elements agree within the errors,

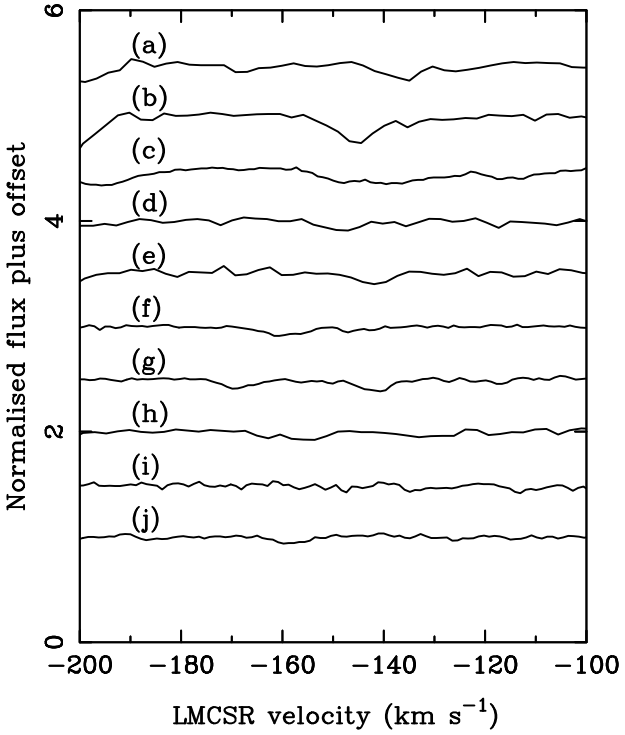

Figure 5. Spectra for sightlines with components with LMC standard of rest less than –130 km s^{-1}. The ordinate is normalised flux plus an offset in incrments of 0.5. The abscissa is the LMCLSR. (a) SK-67 199 (b) SK-70 111 (c) HDE 269702 (d) SK-69 274 (e) SK-66 118 (f) SK-67 38 (g) LH10 0361 (h) SK-66 5 (i) SK-70 69 (j) SK-66 171.

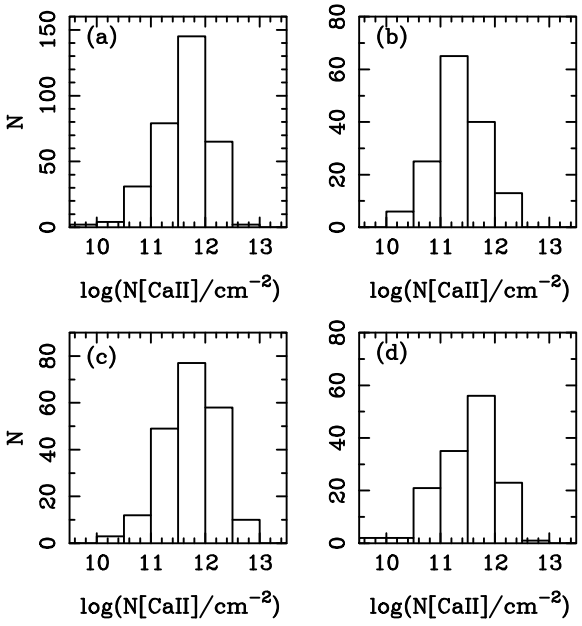

Figure 6. Histogram of Ca II column densities for components derived from the FEROS and UVES spectra. Low-column density bins are severely affected by S/N ratio effects. (a) LV gas $v < +40$ km s^{-1} (b) $+40 \leq v \leq +100$ km s^{-1} (c) $+100 \leq v \leq +150$ km s^{-1} (d) $v > +150$ km s^{-1}.

providing evidence that at least in these cases the Ca II and H II sample the same phase of the interstellar medium. The discrepant case is towards SK-69 214 where the velocities are different by 5.4 km s^{-1}, although low S/N ratio in the H I observations.

4.1.3 Variation of LMC I/HVC Ca II column density with position

Figures A6 and A7 show maps of the Ca II column density as a function of position for the I/HVCs observed towards the LMC, using the column densities derived from FEROS and UVES archival data. The log of the column density ranges from <10.7 cm^{-2} (a 3σ upper limit for SK-67 14 at l, b=278.27°,–36.05°) to 12.50 cm^{-2} (SK-69 214 at l, b=277.99°,–31.84°) for the integrated flux between +40 and +60 km s^{-1}, and from <10.7 cm^{-2} (a 3σ upper limit for SK-67 2 at l, b=278.36°,–36.79°) to 12.16 cm^{-2} (SK-68 114 at l, b=278.90°,–32.35°) for the integrated flux between +60 and +100 km s^{-1}.

Fig. 6 shows a histogram of the Ca II column densities observed towards the FEROS and UVES targets. For intermediate-velocity gas with LSR velocities between +40 and +100 km s^{-1} the column density ranges from 10.94 to 12.50 dex with median value of 11.25 dex (N=50), compared with 11.0 to 12.4 (median=11.5 dex, N=18) in Ben Bekhti et al. (2008). For gas with velocities between +100 and +150 km s^{-1} the range is from 11.01 to 12.31 dex (median=11.51 dex), compared with 11.0 to 12.4 dex (median=11.5 dex, N=18) in Ben Bekhti et al. This compares with low-velocity Galactic gas in the current sample that has column densities ranging from 10.93 to 12.58 dex with median value of 11.82 dex (N=97), compared with 10.9 to 12.6 (median=11.8 dex, N=16) for the corresponding velocities in Ben Bekhti et al., and median of 11.63 dex (N=362) towards low-velocity gas observed by Smoker et al. (2003).

4.1.4 The Ca II/H I, Ca II/Ca I, Ca II/O I, Ca II/Na I and Na I/H I ratios for LMC I/HVCs

Table 3 shows 21 stars for which more than one species was detected in Ca II, Na I, O I, Fe II or H I. In only six of the sightlines are both Ca II and 21-cm H I detected, with values of $\log[N(\mathrm{Ca\,II})/N(\mathrm{H\,I})]$ ranging from –6.81 to –7.46. Five of the points lie on the best fit of I/HVCs studied by Wakker & Mathis (2000). However, in the IVC toward SK-69 59, which has $\log N(\mathrm{H\,I})$=18.89, the observed value of $\log[N(\mathrm{Ca\,II})/N(\mathrm{H\,I})]$ of –6.89 is +0.39 dex higher than predicted by Wakker & Mathis, who found that generally halo gas has larger $N(\mathrm{Ca\,II})/N(\mathrm{H\,I})$ ratios than disc gas. In any event, the nine data points shown in Fig. 7 follow the well-known trend that the gas-phase abundance of Ca II decreases with increasing H I column density, as ions are removed from the gas phase and onto dust grains. In their sightline towards SN1987A, Welty et al. find slightly lower ratios of $\log(\mathrm{Ca\,II/H_{tot}}) = -7.2$ to –7.8 for clouds with +100 to +225 km s^{-1}, with LMC features having corresponding ratios from –7.8 to –9.1. In our current sample we did not detect Ca I in any of our FEROS sightlines, with S/N ratios

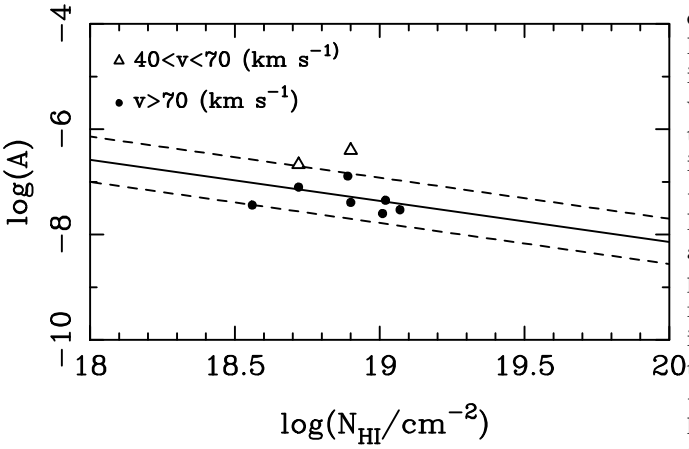

Figure 7. Ca II/H I ratio for FEROS and UVES sightlines with a detection in both species. The solid and dashed lines are the fit from Wakker & Mathis (2000) and the associated RMS.

of typically 50 to 90, with corresponding 5σ column density upper limits of ∼10.5 to 10.2 dex. The ratio of Ca II to Ca I therefore exceeds 1.5 dex towards the HVC SK-69 59 and 2.1 towards IVC SK-69 214. Finally, we note that Lehner et al. (2009) find an average metallicity in their 139 LMC sightlines of [O I/H I]=–0.51, indicating a sub-solar metallicity for the HV gas and similar to that of the LMC which has Fe/H of ∼0.5 dex (e.g. Bertelli et al. 1992, Carrera et al 2008).

The Ca II/O I ratio can be used to estimate the amount of dust present in the LMC HVCs. By studying two halo sightlines, Richter et al. (2009) found HVCs with N(Ca II)/N(O I) similar to the solar Ca/O abundance ratios, indicating that those clouds do not contain significant amounts of dust. However, in the diffuse ISM, depletion onto dust grains causes the value of Ca/O to be frequently more than 1.5 dex lower than the solar value. Comparing the current dataset to that of Lehner et al. (2009), we find values of N(Ca II)/N(O I) of <–3.39 for SK-67 256, –3.38 or –3.64 (depending on whether we count one or both Ca II components) for SK-68 111, –3.66 for HD 269599, –3.06 for SK-69 50, –3.37 for SK-66 100, –3.46 for SK-67 168, –3.88 for SK-67 38, –3.09 for SK-70 60, –3.76 for SK-70 69 and –2.57 or –2.90 (depending on whether we count one or both Ca II components) for SK-70 78. Given the solar abundances $(O/H)_\odot$=–3.31 (Asplund et al. 2004) and $(Ca/H)_\odot$=–5.65 (Morton 2003, 2004), the solar Ca/O ratio is –2.34, hence one of the current sightlines appears to be lightly depleted, with the other nine showing depletions of ∼1 dex. This suggests the presence of dust grains, although we have made no ionisation corrections, and in the diffuse ISM Ca II is a trace species with the majority of the calcium being in the form of Ca III (Sembach et al. 2000). Nonetheless, the presence of dust is also indicated in some of the sightlines studied by Lehner et al. (2009) that have sub-solar Si II/S II ratios, in agreement with the current result.

In common with earlier work (Routly & Spitzer 1952, Siluk & Silk 1974, Vallerga et al. 1993), the ratio of Ca II/Na I D is found to increase markedly as one moves to high velocities, with the vast majority of sightlines only showing HVC absorption in Ca II K and not in Na I D, although with some exceptions (e.g. Richter et al. 2009). In extragalactic sightlines the effect is less clear, with Richter et al. (2011) finding a range from –0.66 to 1.36, again typical of the diffuse warm interstellar medium. They note that in these conditions where the electron densities are less than ~ 0.05 cm^{-3}, in dust-free gas the Ca II/Na I ratio is roughly constant at +1.6 (c.f. Crawford 1992). In the current sightlines the velocities of the two species are similar, which may be taken as evidence that the two species originate within the same physical region. The same appears to be the case for the very few sightlines in the current sample that show both species in absorption, as displayed in Fig. 8. In the current sample, the only detections of Na I D at LSR velocities exceeding +40 km s^{-1} (excluding the LMC and SMC) are: at ∼+68 km s^{-1} with column density ratio $\log[N(\mathrm{Ca\,II})/N(\mathrm{Na\,I})]$= –0.44±0.05 dex) and ∼+110 km s^{-1} with column density ratio $\log[N(\mathrm{Ca\,II})/N(\mathrm{Na\,I})]$=+0.41±0.20 dex) towards LHA 120-S 93; a borderline detection at ∼+68 km s^{-1} towards SK-69 214 with $\log N$(Na I)=10.38 cm^{-2} but with no Ca II detected at the same velocity; at ∼+45 km s^{-1} towards SK-70 111 with $\log N$(Ca II)=12.11 cm^{-2} and $\log N$(Na I)=10.98 cm^{-2} (a ratio of 1.13±0.07 dex); and finally at ∼+135 km s^{-1} towards AzV 483 in the LMC. For high velocity gas, the maximum observed lower limit to the Ca II/Na I ratio is towards SK-67 112, where $\log[N(\mathrm{Ca\,II})/N(\mathrm{Na\,I})]$>1.45 dex in the feature at 101.8 km s^{-1}. For intermediate velocity gas, the maximum ratio is toward SK-69 237 where $\log[N(\mathrm{Ca\,II})/N(\mathrm{Na\,I})]$>1.58 dex.

For gas with absolute LSR velocities exceeding 40 km s^{-1}, Ben Bekhti et al. (2008) have five detections of both Ca II and Na I D, which have Ca II/Na I ratios of –0.2 (complex L), 0.4, 0.4 (Magellanic Stream), 0.5 and 1.4 dex (other gas). In extra-planar gas van Loon et al. (2009) find a ratio of +0.4 dex with a range from 0.23 to 0.56 dex, which is typical of low-velocity components measured by Welsh et al. (2009) and Smoker et al. (2015). We note that for IVCs with a Ca II/Na I ratio exceeding 5 the gas is characterised as having a temperature of ∼10,000 K and at least partially ionised (e.g Hobbs 1975, Welsh et al. 2009). Lower values of this ratio are found in denser and cooler clouds.

We only have upper limits to the Na I/H I ratios in the current sample. These are $\lesssim$8.3 dex at an H I column density of 19.0 dex, compared with the best-fit line from Wakker & Mathis that predicts an abundance ratio of ∼8.1 dex at this H I column density. This may be related to beam-smearing for the H I observations that we use. Higher S/N observations would likely detect Na I in these sightlines.

We have decided not to include Cloudy because the Ca II and Na I may not be physically associated with the H I (a fact that Cloudy assumes is the case), and hence the derived ionisation correction using a Cloudy model will likely be incorrect. See Fox et al. (2013) for a discussion.

4.1.5 FEROS and UVES SMC sightlines

Eighty seven sightlines are present in the current sample towards the SMC. As the SMC has a recessional LSR velocity of ∼+160 km s^{-1}, the separation of the HVC and SMC components is not as marked as in the LMC. The Ca II column density ranges from <10.7 cm^{-2} to 11.6 cm^{-2} for the integrated flux between +60 and +100 km s^{-1}.

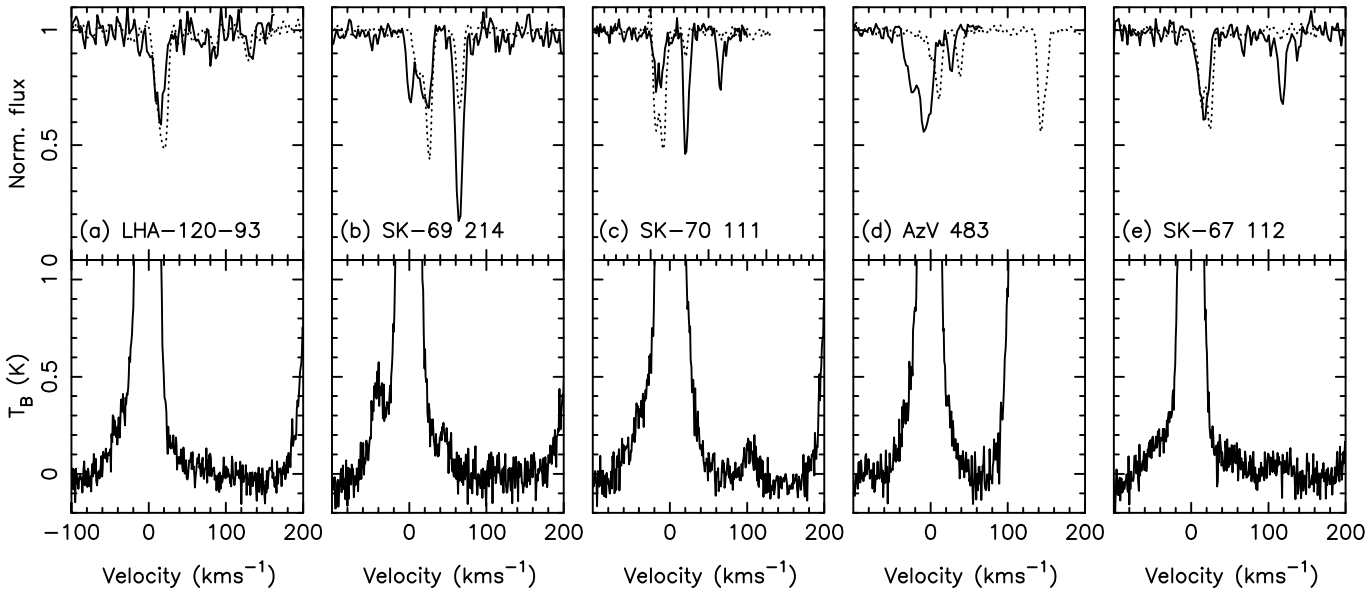

Figure 8. (a)-(d) Ca II K, Na I D and H I LAB and GASS spectra of sightlines with possible Na I I/HVC detections. (e) Corresponding spectra with high Ca II/Na I ratio. Filled lines in the top panel are Ca II with dashed lines being Na D1.

4.2 Small-scale spatial structure of I/HVCs towards the LMC and SMC from FLAMES-GIRAFFE observations

Non-Magellanic Ca II K absorption is detected at intermediate- or high-velocities in many sightlines. The minimum star-star distance is 11 arcsec and the maximum is 27 arcminutes. Figure 9 shows the *composite* Ca II K spectra towards the four clusters, formed by median-combining the individual normalised spectra. The spectra have been boxcar smoothed using a box of three pixels, which retains the full spectral resolution as the FWHM of emission features measured from the arc frames is four pixels. For NGC 330 the composite spectrum S/N ratio in the boxcar smoothed spectrum is ∼500, being ∼1100 for NGC 346, ∼1200 for NGC 1761 and ∼1200 for NGC 2004. Also shown in Fig. 9 are the GASS and LABS survey 21 cm H I spectrum towards both clusters. These data are presented simply to confirm the weakness in H I of the I/HVC emission – in the GASS and LAB spectra no such emission is seen.

An immediate question to ask is whether the observed absorption at I/HVC velocities could be stellar in nature. Figure 10 shows an example of a star in NGC 2004 where strong I/HVC Ca II absorption is detected at observed (raw) velocities of +63 and +116 km s^{-1}. The FWHM of these lines is ∼17 km s^{-1} (most or all of which is caused by instrumental broadening of ∼16 km s^{-1}), compared to the width of the N II stellar line at 3995Å of ∼60 km s^{-1}. The narrowness of these I/HVC components implies they are circumstellar or interstellar rather than stellar. Furthermore, the fact that I/HVC features are observed at similar LSR velocities in both the Ca K and H I lines where the latter is detected (Figs. 11 and 12) toward many different stars is very difficult to explain if these lines are circumstellar, since in that case the velocities would vary with the velocity of the star.

We now briefly discuss the Ca II K absorption line components toward the four individual Magellanic Cloud clusters observed with FLAMES-GIRAFFE.

4.2.1 NGC 330 (SMC)

The sightlines toward NGC 330 (Figs. 3a and A8) in the SMC show Ca II absorption at intermediate velocities between ∼+60–80 km s^{-1}, well separated from both the low velocity and SMC gas. Peak Ca II equivalent widths at IVC velocities are ∼80 mÅ, with many sightlines having values of ∼60 mÅ. A number of sightlines show *no* corresponding Ca II absorption with a S/N ratio of ∼60, which following Eqn. 2 gives a 3σ upper limit on the equivalent width of ∼10 mÅ, given that the instrumental resolution ($\Delta\lambda_{\rm instr}$) is 0.21Å for the GIRAFFE HR2 setting and assuming an unresolved component, viz:

$$EW_{\rm lim}(X) = 3 \times ({\rm S/N})^{-1}_{\rm cont} \Delta\lambda_{\rm instr}, \quad (2)$$

Hence the variation in the Ca II equivalent width for IVC components exceeds a factor of ∼8 (∼0.9 dex) over the face of the cluster. The velocity map in Fig. A8 shows no obvious large-scale structure or gradients, although clumps of gas at higher central velocities are for example present at (l, b)∼(302.5°,–44.6°) with central velocities some ∼20 km s^{-1} higher than towards the cluster core at (l, b)∼(302.4°,–44.7°) which is a transverse distance of ∼150 pc at the distance of the SMC.

4.2.2 NGC 346 (SMC)

Although I/HVC absorption is visible in many of the FLAMES NGC 346 sightlines (Fig. 3b), the gas merges into

Table 3. Measurements of I/HVC absorption in sightlines in common with Lehner et al. (2009) from which the O I, Fe II and H I data are taken. Components in Ca II K and Na I D are shown when their velocity is greater than +40 km s^{-1}. Components from Lehner et al. (2009) are shown when the velocity is from +90 to +175 km s^{-1}. Sightlines are ordered by increasing RA.

Star	v(O I) (km s^{-1})	log$N$(O I) (cm^{-2})	v(Fe II) (km s^{-1})	log$N$(Fe II) (cm^{-2})	v(H I) (km s^{-1})	log$N$(H I) (cm^{-2})	v(Ca II) (km s^{-1})	log$N$(Ca II) (cm^{-2})	log$N$(Na I) (cm^{-2})
SK-69 43	–	–	–	–	143.6±1.3	19.02±0.06	142.7±0.3	11.67±0.11	<10.66
SK-67 28	–	<14.28	–	<13.19	–	<18.47	–	<11.32	<10.26
SK-68 26	–	–	–	<13.62	–	<18.47	–	<11.32	<10.36
SK-69 59	175.9±0.6	15.06±0.02	173.4±1.3	13.79±0.03	172.4±2.5	18.89±0.11	170.4±0.4	12.00±0.02	<10.56
SK-68 41	–	<13.92	–	–	–	<18.47	–	<11.56	<10.48
SK-66 106	–	<14.63	–	–	–	<18.47	–	<11.38	<10.36
SK-67 150	–	<14.39	–	–	–	<18.47	–	<11.16	<10.38
SK-67 169	–	<14.11	–	–	–	<18.47	83.5±1.0	11.01	(stellar)
”	–	–	–	–	117.4±1.8	18.93±0.08	–	<10.89	<10.24
SK-70 78	97.2±4.4	14.27±0.15	–	–	–	<18.44	78.5±4.9	11.43	<10.38
”	–	–	–	–	–	”	91.4±0.5	11.37	<10.38
HD 269599	119.7±3.4	15.20±0.08	110.6±1.6	13.99±0.05	119.3±5.2	19.07±0.09	117.4±0.7	11.54±0.03	<10.56
SK-71 42	–	–	–	–	66.8±2.3	18.72±0.14	66.0±0.2	12.05±0.04	<10.45
LHA-120 116	–	–	–	–	114.9±1.2	19.11±0.07	115.9±1.1	11.66±0.18	<10.49
SK-68 111	109.6±3.8	15.15±0.11	102.4±1.4	14.35±0.05	–	–	96.1±1.1	11.41±0.03	<10.48
”	–	–	–	–	114.54±3.8	19.01±0.06	114.6±1.2	11.51±0.03	<10.48
SK-69 214	–	–	–	–	43.9±2.0	18.90±0.09	49.3±0.2	12.50±0.06	11.60±0.02
SK-69 274	–	–	–	–	100.1±3.2	18.56±0.20	102.3±0.8	11.12±0.08	<10.36
SK-70 111	–	–	–	–	103.1±1.9	18.72±0.11	104.6±0.4	11.62±0.06	<10.36
	–	–	–	–	–	–	116.5±1.9	11.10±0.29	<10.36
SK-67 256	144.7±1.7	14.95±0.03	138.6±1.4	13.67±0.04	141.0±6.0	18.64±0.13	–	<11.56	(stellar)
SK-68 171	–	<14.46	–	–	–	<18.47	79.3±0.4	11.66	<10.56
SK-70 120	–	–	–	<13.36	–	<18.47	–	<11.32	<10.56
SK-68 63	–	–	–	–	–	–	100.4±0.1	11.17±0.17	<10.19
”	–	–	–	–	–	–	136.1±0.7	10.38±0.18	<10.19
”	–	–	–	–	–	–	152.1±0.2	11.10±0.17	<10.19
SK-65 47	–	–	–	<12.80	–	<18.47	47.9±0.6	11.39±0.17	<10.36
SK-65 47	144.1±4.9	14.04±0.10	–	<12.80	–	<18.47	145.7±0.4	10.94±0.17	<10.36
BI 128	–	<14.49	130.8±2.5	14.04±0.05	–	<18.61	132.1±0.8	11.06±0.30	<10.66
”	–	<14.49	–	–	–		178.7±1.7	11.06±0.30	<10.66
SK-66 18	–	–	–	<13.29	–	<18.47	165.6±0.0	11.51±0.17	<10.34
SK-66 100	107.3±3.1	14.59±0.06	109.6±1.4	13.74±0.04	–	<18.48	109.2±1.7	11.22±0.18	<10.34
	–	–	–	–		–	120.4±0.4	10.87±0.18	<10.34
SK-67 168	110.5±2.6	15.00±0.06	114.5±1.3	14.13±0.03	–	<18.55	108.9±0.5	11.54±0.17	10.87±0.18
”	–	–	–	–	–	–	119.3±0.6	10.74±0.17	<10.49
	–	–	–	–	–	–	132.3±0.3	11.36±0.18	<10.49
BI 237	–	–	109.6±3.0	14.01±0.05	–	<18.62	103.6±0.8	11.29±0.17	<10.58
	–	–	–	–	–	–	131.1±0.6	11.21±0.17	<10.58
SK-67 38	125.2±2.9	14.23±0.10	128.1±2.0	13.47±0.08	–	<18.44	126.4±1.0	10.35±0.30	<10.58
SK-67 05	–	–	112.3±3.6	13.79±0.06	–	<18.63	119.2±0.9	10.25±0.17	–
”	–	–	–	–	–	–	132.5±1.0	10.89±0.17	–
BI 253	–	–	–	<13.36	–	<18.47	107.1±1.0	11.05±1.07	<10.49
SK-68 52	–	<14.26	–	<13.12	–	<18.47	–	–	–
SK-69 50	147.9±0.9	15.42±0.02	145.3±1.2	14.39±0.03	146.9±3.8	19.23±0.10	142.1±0.9	11.62±0.18	<10.55
	–	–	–	–	–	–	148.1±0.0	11.38±0.17	<10.55
SK-70 60	123.3±1.1	14.64±0.07	128.7±1.7	13.79±0.06	–	<18.45	122.7±0.3	11.55±0.17	–
SK-70 69	120.5±2.9	14.71±0.07	108.7±1.7	13.63±0.07	–	<18.48	111.9±0.6	10.95±0.18	<10.49

the SMC material. Hence we do not comment on the variation in these components. The highest velocity gas (presumably tracing the SMC itself) shows a huge variation in absorption-line strength and number of components. This is likely explained by the cluster having a finite depth within the SMC.

4.2.3 NGC 1761 (LMC)

NGC 1761 (LH09) is an LMC cluster that displays two apparently discrete Ca II absorption-line components in its interstellar spectra, well-separated in velocity, which are not at Milky Way or LMC velocities (Figs. 3c, A9 and A10). One is an IVC at ∼+90 km s^{-1} with a maximum equivalent width of ∼100 mÅ, and the other is an HVC at ∼+160 km s^{-1} with a maximum equivalent width of ∼40 mÅ. One sightline shows no Ca II absorption at either of these two ve-

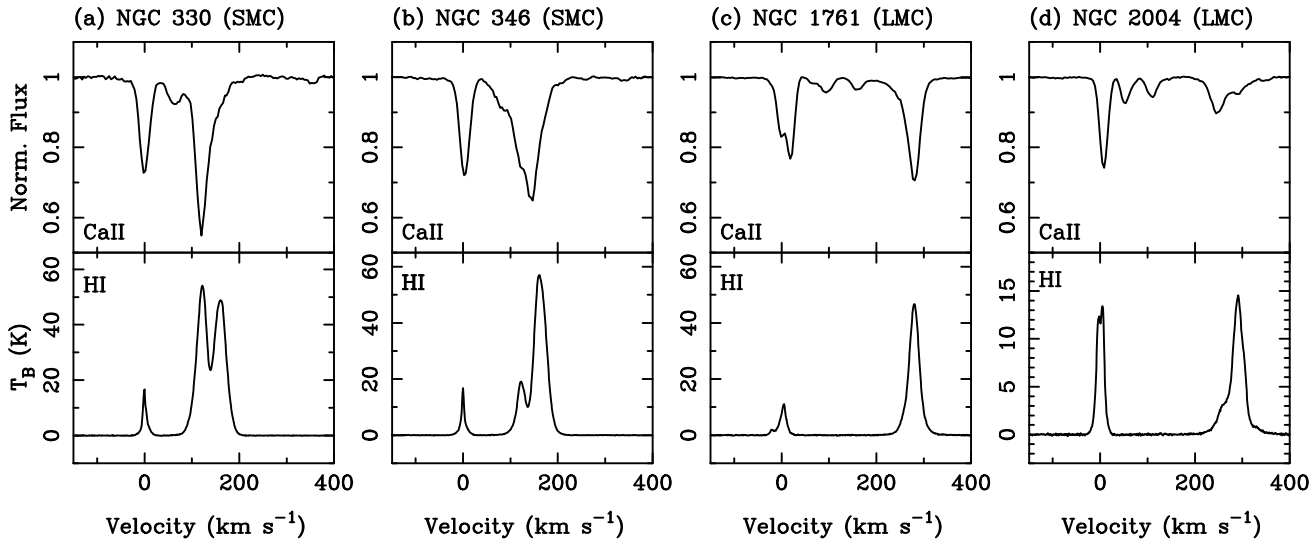

Figure 9. Ca II K composite GIRAFFE spectra and H I GASS and LABS survey spectra for four clusters. See Sect. 4.2 for details.

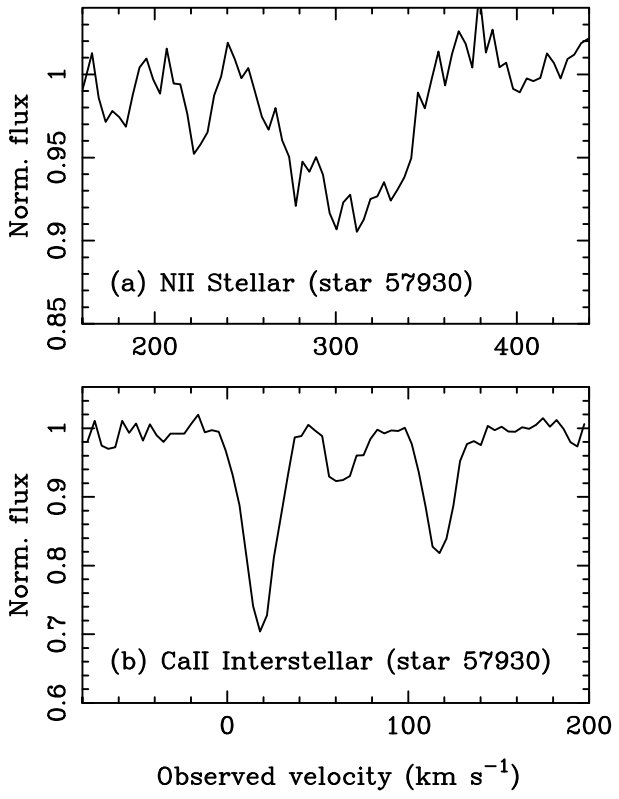

Figure 10. FLAMES-GIRAFFE spectra of star 57930 in NGC 2004 (LMC). (a) Stellar absorption line of N II (3995Å) with FWHM∼60 km s^{-1} (b) Absorption lines around Ca II K (3933Å). The profiles uncorrected for instrumental broadening of ∼16 km s^{-1} have FWHM∼17–19 km s^{-1}, implying that the lines are narrow (possibly unresolved) and hence interstellar or circumstellar rather than stellar.

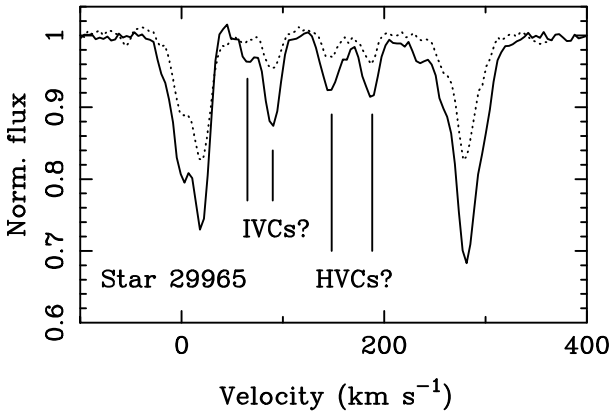

Figure 11. Two-component FLAMES-GIRAFFE Ca II absorption-line structure in the I/HVCs towards NGC 1761 in the LMC. The full line is for Ca K and the dotted line for Ca H.

locities, in data with a S/N ratio of ∼90, corresponding to a 3σ equivalent width upper limit of 7 mÅ. Thus the Ca II equivalent widths vary across the cluster by factors of >14 (IVC gas) and >6 (HVC gas). NGC 1761 is hence the cluster in which the biggest variation in Ca II absorption-line strength is seen in the current sample. As in the FEROS and UVES data, there are hints of two-component velocity structure towards a handful of sightlines, examples being shown in Fig. 11. The velocities of the gas in Fig. **??** for the IVC between +30 and +105 km s^{-1} show a transverse gradient of ∼20 km s^{-1} moving from east to west in Galactic longitude. Between +125 and +200 km s^{-1}, two clumps of gas are present (c.f. Fig. 11, with the lower velocity clump to the East centred on l, b∼277.1°,–36.05°) having velocities from ∼+140–150 km s^{-1} and the structure to the west showing a larger variation in velocity.

4.2.4 NGC 2004 (LMC)

NGC 2004 in the LMC shows the most complexity in intermediate- and high-velocity gas among the four clusters studied, with at least three I/HVC components visible in Ca II, at ∼+60, ∼+120 and ∼+150 km s^{-1}, the latter two components sometimes being merged at the FLAMES resolution (Figs. 3d, 3e, A11 and A12). The peak equivalent widths in the first two components are 36 and 63 mÅ, which are ∼5 and ∼9 times stronger than the 3σ upper limits in the cases where no I/HVC gas is detected in Ca II absorption. As in the FEROS and UVES data, there are hints of two-component velocity structure towards a few sightlines, an examples being shown in Fig. 12.

4.2.5 Summary of observed I/HVC EW variations

EW variations in Ca II for Magellanic Cloud I/HVCs exceed a factor of 10 (or ∼1 dex in column density) on transverse scales as small as ∼5 pc, assuming that the clouds lie at a distance of ∼55 kpc. If the clouds are in the halo of the Milky Way then the transverse scales would be reduced accordingly. These variations are large but not compared to previous work on the M 15 IVC by Meyer & Lauroesch (1999) and Welsh et al. (2009), who found column density variations of a factor exceeding 10 in IVC gas on scales of <0.1 pc. In the Galactic ISM, variations of up to 2 dex are also present on AU to pc scales in Na I (Welty & Fitzpatrick 2001; Points, Lauroesch & Meyer 2004; Lauroesch 2007 and references therein; van Loon et al. 2009; Welsh et al. 2009 amongst others). Similarly, Appendix 15 of Wakker (2001) assumes a factor 2 in variation caused by H I small-scale structure, factors of 1.5 (Ca II) and 2.5 (Na I) to account for variations in depletion and further factors of 2 (Ca II) and 6 (Na I) for ionisation variations. Typically, then, pc-scale variations in Ca II and Na I are of the order 0.8 dex and 1.5 dex, respectively, which is in line with the current work. The fact that in Milky Way extra planar gas, these variations exist in material far away from supernova remnants, has been taken to imply that this small-scale structure is either continuously regenerated or persists for long periods of time (e.g. van Loon et al. 2009, although see Marasco & Fraternali 2011).

We have analysed the variations in Ca II equivalent width towards three clusters observed with FLAMES/GIRAFFE in a total of five velocity ranges. Figure A13 shows the percentage difference in equivalent width plotted against the distance between the stellar sighlines, with the derived upper limits shown in open circles with the measurements being filled circles. Table 4 shows the derived mean, median and standard deviation of the variaion in the equivalent width values at a range of velocities. Towards NGC 2004 the variation in the high velocity component is typically a 50 to 100 percent larger than to the intermediate velocity component. This is naturally explained by the HVC being further away than the IVC and hence only the larger scales being sampled in the HVC. However, the same behaviour is not seen towards the I/HVC components towards NGC 1761. Likewise, there is no clear increase in scatter in the equivalent width for any of the clusters as the scales sampled increase from 0.05 to 0.4 degrees.

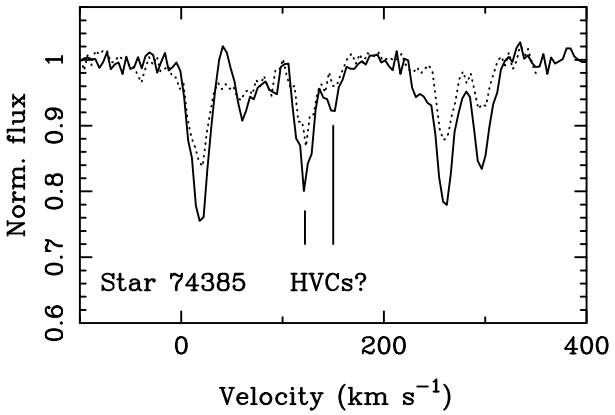

Figure 12. Two-component FLAMES-GIRAFFE Ca II absorption-line structure in the I/HVCs towards NGC 2004 in the LMC. The full line is for Ca K and the dotted line for Ca H.

FLAMES-GIRAFFE observations of the Tarantula nebula have been presented in Na I by van Loon et al. 2013, who find that the standard deviation in equivalent width in the LMC gas is of the order of 25 percent, being 7 per cent for the Milky Way gas. The relative variation in Na I absorption as a function of angular sky separation increases from ∼0.50 at 10 arcsecond separation to 0.65 at 100 arcseconds, although with correlation coefficient of only 0.27.

Similarly, Van Loon et al. (2009) and Smoker et al (2015) found variations in the Ca II equivalent width in low velocity gas of ∼10 per cent on scales of ∼0.1, a factor of ∼10 smaller than seen in the current I/HVC sightlines. These fluctuations were explained by a simple model of the ISM comprised of spherical clouds of radii between 1 AU and 10-pc with filling factor of ∼0.2 (van Loon et al. 2009 Appendix B). Due to the limited spatial resolution of our study (scales probed from around 5-pc to 500-pc assuming the clouds are at the distance of the Magellanic Clouds) we cannot use these observations to say much about the size of the clouds although from the lack of detection of I/HVC in adjacent FLAMES-GIRAFFE fibres it is clear that the filling factor is somewhat less than unity.

4.3 Search for molecular gas towards and in the LMC in FLAMES spectra

Claims of molecular hydrogen detections in I/HVCs towards the LMC have been put forward by Richter et al. (1999) and Bluhm et al. (2001) using ORFEUS (Orbiting Retrievable Far and Extreme Ultraviolet Spectrometer) data. Additionally, Richter et al. (2003) obtained FUSE observations towards the LMC star Sk -68 80 and found IVC absorption at ∼+50 km s^{-1} for 30 transitions and hints of molecular Hydrogen at HVC velocities of ∼+120 km s^{-1}, although being "too weak to claim a firm detection". Additionally, towards the LMC star Sk -68 82, Richter et al. (2003) co-added 15 H_2 transitions and found molecular gas at IVC and HVC velocities, although noting that the stellar continuum is very irregular which complicates the interpretation of the lines observed. Re-ananalysis of this star by Lehner et al. (2009)

Table 4. Percentage variation in observed Ca II equivalent width for I/HVCs in the FLAMES sample as a function of star-to-star separation for three Magellanic clusters.

Cluster	velocity range ($km\,s^{-1}$)	Separation (arcmin)	EW_{Med} variation (percent)	EW_{Ave} variation (percent)	EW_{sigma} variation (percent)
NGC 330	45 to 85	0.05 to 0.10	64.2	98.0	104.4
NGC 1761	60 to 120	"	63.2	101.4	118.5
NGC 1761	130 to 190	"	69.6	127.6	156.5
NGC 2004	40 to 100	"	51.6	78.0	83.0
NGC 2004	100 to 180	"	108.4	174.8	193.9
NGC 330	45 to 85	0.10 to 0.15	63.4	103.9	121.4
NGC 1761	60 to 120	"	73.1	121.8	158.2
NGC 1761	130 to 190	"	97.4	148.7	161.7
NGC 2004	40 to 100	"	60.5	90.6	94.4
NGC 2004	100 to 180	"	56.7	108.4	193.0
NGC 330	45 to 85	0.15 to 0.20	71.7	113.5	133.6
NGC 1761	60 to 120	"	76.8	139.4	189.2
NGC 1761	130 to 190	"	98.6	146.9	165.1
NGC 2004	40 to 100	"	64.7	100.1	136.7
NGC 2004	100 to 180	"	110.2	179.7	216.0
NGC 330	45 to 85	0.20 to 0.25	75.4	102.4	100.7
NGC 1761	60 to 120	"	112.0	172.6	199.1
NGC 1761	130 to 190	"	88.7	144.3	148.7
NGC 2004	40 to 100	"	64.2	111.2	136.7
NGC 2004	100 to 180	"	112.3	183.2	236.7
NGC 330	45 to 85	0.25 to 0.30	49.1	102.2	190.4
NGC 1761	60 to 120	"	124.7	211.2	240.6
NGC 1761	130 to 190	"	95.3	156.6	182.1
NGC 2004	40 to 100	"	109.8	151.1	159.0
NGC 2004	100 to 180	"	104.7	157.5	176.5
NGC 330	45 to 85	0.30 to 0.35	42.2	72.1	78.1
NGC 1761	60 to 120	"	236.2	348.2	148.7
NGC 1761	130 to 190	"	92.0	123.5	98.3
NGC 2004	40 to 100	"	163.5	224.0	182.0
NGC 2004	100 to 180	"	315.6	259.0	168.7
NGC 330	45 to 85	0.35 to 0.40	52.5	69.3	65.0
NGC 1761	60 to 120	"	571.8	537.8	463.0
NGC 1761	130 to 190	"	55.3	72.4	82.1
NGC 2004	40 to 100	"	–	–	–
NGC 2004	100 to 180	"	–	–	–
NGC 330	45 to 85	0.40 to 0.45	47.3	38.2	22.4
NGC 1761	60 to 120	"	–	–	–
NGC 1761	130 to 190	"	–	–	–
NGC 2004	40 to 100	"	–	–	–
NGC 2004	100 to 180	"	–	–	–

found no HVC detection in H_2. Likewise, although observations by André et al. (2004) towards the Magellanic clouds using FUSE, HST and VLT observations have also shown the presence of H_2, HD and CO molecules, these detections were only at IVC, Milky Way or LMC/SMC velocities, with nothing seen corresponding to HVC gas. Searches for CO in emission towards HVCs have generally only given upper limits, (e.g. Dessauges-Zavadsky, Combes & Pfenniger 2007), possibly due to the fact that small filaments of gas are unable to provide sufficient shielding from the ambient UV field (Richter et al. 2003). Overall, the presence of molecular gas in Magellanic HVCs is still a subject of debate.

Figures 13 and 14 show GIRAFFE spectra towards NGC 1761 and NGC 2004 in the molecular lines CH^+ (4232Å) and CH (4300Å). Tentative absorption in one or both of these species is detected in only three sightlines towards NGC 1761 and one towards NGC 2004 at the LMC velocity, with no absorption detected at Galactic or I/HVC velocities. We note that due to the relatively low gas density in HVCs, the detection of CH and CH^+ (although not H_2) is a-priori unlikely in equilibrium conditions. Na I is rarely seen in absorption in HVCs, and CH is very well correlated with Na I in the range $\log(N(\mathrm{Na\,I})\ \mathrm{cm}^{-2})$∼12.2-14.2 (Smoker et al. 2014).

The maximum equivalent widths measured in CH^+ (4232Å) are 12.4 mÅ for NGC 1761 and 6.3 mÅ for NGC 2004, respectively. For CH (4300Å), the corresponding values was 4.7 mÅ for NGC 1761 with no obvious CH detection towards NGC 2004. Towards NGC 1761 a few of our sightlines have S/N ratios exceeding 400, which leads to a 3σ detection limit of 1.7 mÅ or a EW variation exceeding ∼7 on scales of ∼10 arcminutes.

Our detection rate is much lower than in the UVES spectra of Welty et al. (2006), who found either CH and/or CH^+ in 9 out of 13 LMC stars observed with UVES, likely due to the lower S/N ratio in many of our sightlines. However, the observed equivalent widths in the two samples are similar, with Welty et al. finding EWs from 0.5 to 13.0 mÅ for CH^+ (4232Å) and 0.8 to 10.5 mÅ for CH (4300Å).

Finally we note that the absence of a strong molecular component in the LMC HVCs is consistent with the clouds being predominantly ionised and of a similar type to those studied by Lehner et al. (2009) using FUSE UV spectra. They found a lack of H_2 and a high ionisation level (average hydrogen ionization fraction >50%), with ≈90% of their sightlines also showing O VI, indicating a diffuse, high-temperature component.

5 SUMMARY

We have presented FEROS and FLAMES optical absorption line observations of intermediate and high velocity clouds toward target stars within clusters in the LMC and SMC. IVC or HVC absorption in Ca II K is detected in ∼60 per cent of the FEROS and UVES sightlines and in many of the LMC FLAMES-GIRAFFE sightlines. In the I/HVCs we find a variation in the observed Ca II equivalent width of a factor of ∼10 over ∼10 arcminutes or ∼150 pc at the distance of the LMC. Na I D is only tentatively detected at high velocities in one sightline, indicating the Routly-Spitzer effect. The HV gas towards NGC 2004 displays 50 to 100 percent more small-scale variation than the IV gas, indicating a structural difference between the two types of cloud. However, this is likely caused by the fact that the HV gas is further away and in any case the same difference is not seen towards our other LMC sightline NGC 1761.

In the few sightlines with good H I data the velocities of Ca II and H I are the same within the errors, indicating that the two species are co-spatial. The Ca II/H I ratios are higher in gas with velocities less than 70 $\mathrm{km\,s^{-1}}$ than in HV gas, likewise the sightine with lowest Ca/O ratio is the one with the lowest velocity. These results are consistent with previous work indicating the the metalicities of IVCs tend to be closer to solar than for HVCs. Combining these Ca II observations with O I measurements from the literature, we conclude that dust is present at HVC velocities in the LMC sightlines.

Finally, we detect CH or CH^+ molecular gas in only four sightlines (and only at Magellanic velocities and not in the Milky Way or I/HVC components).

ACKNOWLEDGEMENTS

Data from ESO FEROS programme ID 078.C-0493(A) and FLAMES programme 171.D-0237(B) were taken from the ESO archive. This research has made use of the SIMBAD Database, operated at CDS, Strasbourg, France and the ESO Archive. JVS thanks the ESO Director General Discretionary Fund and Queen's University Belfast Visiting Scientist Fund for financial support. We would like to thank two anonymous referees whose comments significantly improved the paper.

REFERENCES

André M. K., et al., 2004, A&A, 422, 483
Andreani P., Vidal-Madjar A., 1988, Nature, 333, 432
Asplund M., Grevesse N., Sauva, A. J., Allende Prieto C., Kiselman D., 2004, A&A, 47, 751
Bagnulo S., Jehin E., Ledoux C., Cabanac R., Melo C., Gilmozzi R., 2003, ESO Messenger no. 114, Page 10
Ben Bekhti N., Richter P., Westmeier T., Murphy, M. T., 2008, A&A, 487, 583
Ben Bekhti N., Richter P., Winkel B., Kenn F., Westmeier T., 2009, A&A, 503, 483
Bertelli G., Mateo M., Chiosi C., Bressan A., 1992, ApJ, 388, 400
Blades J. C., 1980, MNRAS, 190, 33
Blades J. C., Wheatley J. M., Panagia N., Grewing M., Pettini M., Wamsteker W., 1988a, ApJ, 332, 75
Blades J. C., Wheatley J. M., Panagia N., Grewing M., Pettini M., Wamsteker W., 1988b, ApJ, 334, 308
Bland-Hawthorn J., 2009, IAUS, 254, 241
Blitz L., Spergel D. N., Teuben P. J., Hartmann D., Burton W. B., 1999, ApJ, 514, 818
Bluhm H., de Boer K. S., Marggraf O., Richter P., 2001, A&A, 367, 299
Bregman J. N. 2004, in High Velocity Clouds, eds. H. van Woerden, B. P. Wakker, U. J. Schwarz, K. S. de Boer, Astrophys. Space Sci. Lib., 312, 341
Carrera R., Gallart C., Hardy E., Aparicio A., Zinn R., 2008, AJ, 135, 836
Chiappini C., in Fumes J. G. S. J., Corsini E.M., Eds, ASP Conf. Ser. 2008, Vol. 396, Formation and Evolution of Galaxy Disks, Astron. Soc. Pac., San Francisco, p. 113
Crawford I. A., 1992, MNRAS, 259, 47
Dekker H., D'Odorico S., Kaufer A., Delabre B., & Kotzlowski H., 2000, SPIE, 4008, 534
Dessauges-Zavadsky M., Combes F., Pfenniger D., 2007, A&A, 473, 863
Diamond P. J., Goss W. M., Romney J. D., Booth R. S., Kalberla P. M. W., Mebold U., 1989, ApJ, 347, 302
de Heij V., Braun R., Burton W. B., 2002, A&A, 391, 67
Fox A. J., Wakker B. P., Savage B. D., Sembach K. R., Tripp T. M., & Bland-Hawthorn J. 2005, ApJ, 630, 332
Fox A. J., Wakker B. P., Smoker J. V., Richter P., Savage B. D., Sembach K. R., 2010, ApJ, 718, 1046
Fox A. J., Richter P., Wakker B. P., Lehner N., Howk C. J., Ben Bekhti N., Bland Hawthorn J., Lucas S., 2013, ApJ, 722, 110
Fox A. J., Wakker B. P., Barger K. A., et al., 2014, ApJ, 787, 147
Giovanelli R., 1981, AJ, 86, 1468
Gritton J. A., Shelton R. L., Kwak K., 2014, 795, 99
Heitsch, F., Putman, M. E. 2009, ApJ, 698, 1485
Hobbs L. M., 1975, ApJ, 202, 628
Hopp U., Schulte-Ladbeck R. E., Kerp J., 2007, MNRAS, 374, 1164
Howarth I. D., Price R. J., Crawford I. A., Hawkins I., 2002, MNRAS, 335, 267
Howarth I. D., Murray J., Mills D., Berry D. S., 2003, Starlink User Note SUN 50, Rutherford Appleton Laboratory/CCLRC
Hunter I., Smoker J. V., Keenan F. P., Ledoux C., Jehin E., Cabanac R., Melo C., Bagnulo S., 2006, MNRAS, 367, 1478
Kalberla P. M. W., Burton W. B., Hartmann D., Arnal E. M., Bajaja E., Morras R., Pöppel, W. G. L. 2005, A&A, 440, 775
Kaufer A., Stahl O., Tubbesing S., Nrregaard P., Avila G., Francois P., Pasquini L., Pizzella A., 1999, The Messenger 95, 8
Keller S. C., Wood P. R., 2006, ApJ, 642, 834
Kennicut R. C., 1998, ApJ, 498, 541
Lauroesch J. T., 2007, in Haverkorn M., Goss W. M., eds, ASP Conf. Ser. Vol. 365, Small Ionized and Neutral Structures in the Diffuse Interstellar Medium, Astron. Soc. Pac., San Francisco, p. 40

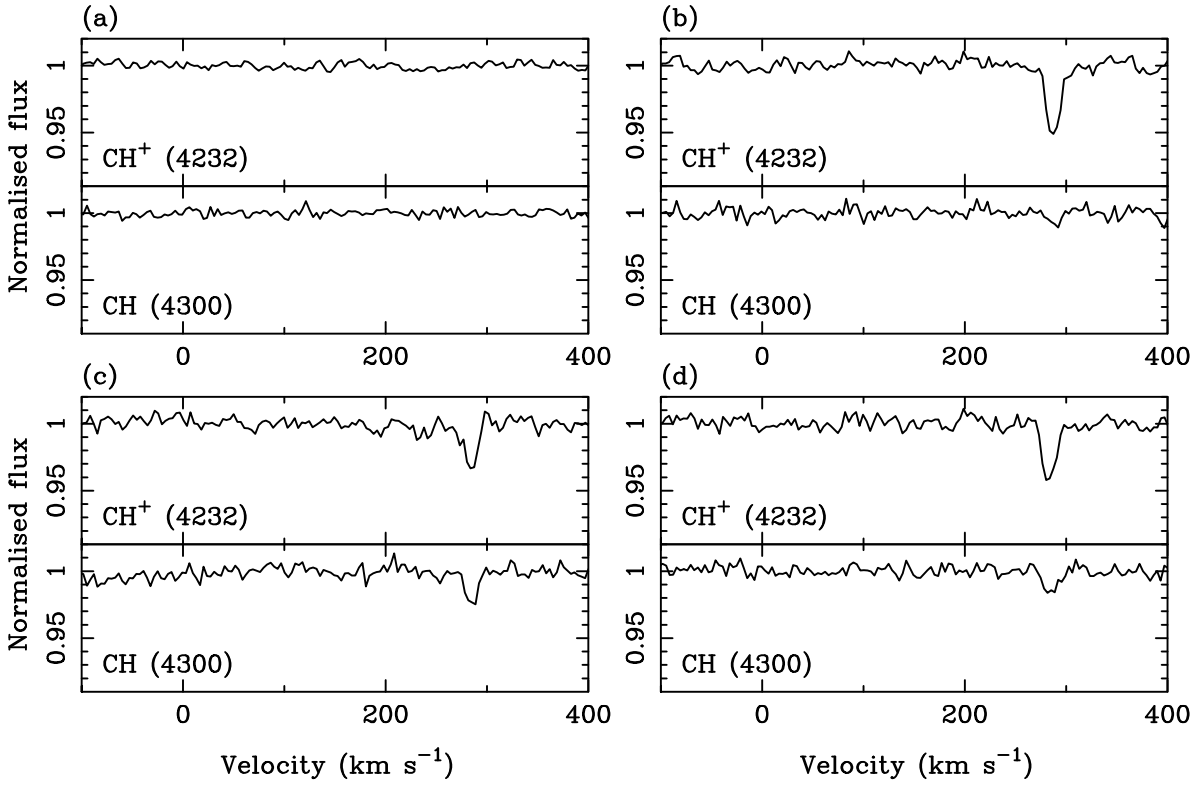

Figure 13. CH^+ (4232Å) and CH (4300Å) profiles towards NGC 1761 taken with FLAMES-GIRAFFE. Only eight sightlines show molecular line absorption at Magellanic Cloud velocities, and none show molecular absorption at Galactic or I/HVC velocities.

Lehner N., Staveley-Smith L., Howk J. C., 2009, ApJ, 702, 940
Lehner N., Howk J. C., 2011, Science, 334, 955
Marasco A., Fraternali F., 2011, A&A, 525, 134
McClure-Griffiths N. M., et al., 2009, ApJS, 181, 398
Meyer D. M., Lauroesch J. T., 1999, 520, 103
Mirabel I. F., 1981, ApJ, 250, 528
Misawa T., Charlton J. C., Kobulnicky H. A., Wakker, B. P., Bland-Hawthorn J., 2009, ApJ, 695, 1382
Molaro P., Vladilo G., Monai S., d'Odorico S., Ferlet R., Vidal-Madjar A., Dennefeld M., 1993, A&A, 274, 505
Morton D. C., 2003, ApJS, 149, 205
Morton D. C., 2004, ApJS, 151, 403
Muller C. A., Oort J. H., Raimond E., 1963, CR Acad. Sci. Paris, 257, 1661
Nasoudi-Shoar S., Richter P., de Boer K. S., Wakker B. P., 2010, A&A, 520, 26
Nidever D. L., Majewski S. R., Burton W. B., 2008, ApJ, 679, 432
Olano C. A., 2004, A&A, 423, 895
Olano C. A., 2008, A&A, 485, 457
Pasquini, L. et al. 2002, The Messenger 110, 1
Pisano D. J., Barnes D. G., Gibson B. K., Staveley-Smith L., Freeman K. C., Kilborn V. A., 2004, ApJ, 610, L17
Points S. D., Lauroesch J. T., Meyer D. M., 2004, PASP, 116, 801
Richings A. J., Schaye J, Oppenheimer B. D., 2010, MNRAS, 440, 3349
Richter P., de Boer K. S., Widmann H., Kappelmann N., Gringel W., Grewing M., Barnstedt J., 1999, Nature, 402, 386
Richter P., Sembach K. R., Howk J. C., 2003, A&A, 405, 1013
Richter P., Charlton J. C., Fangano A. P. M., Bekhti N. B., Masiero J. R., 2009, ApJ, 695, 1631
Richter P., Krause F., Fechner C., Charlton J. C., Murphy M. T., 2011, A&A, 528, 12
Richter P., Fox A. J., Ben Bekhti N., Murphy M. T., Bomans D., Frank S., AN, 335, 92
Routly P. M., Spitzer L., 1952, ApJ, 115, 227
Savage B. D., de Boer K. S., 1981, ApJ, 243, 460
Sembach K. R., Howk C. J., Ryans R. S. I., Keenan F. P., 2000, ApJ, 528, 310
Siegel M. H., Majewski S. R., Gallart C., Sohn S. T., Kunkel W. E., Bran R., 2005, ApJ, 623, 181
Siluk R. S., Silk J., 1974, ApJ, 192, 51
Simon J. D., Blitz L., 2002, ApJ, 574, 726
Smoker J. V., Roger R. S., Keenan F. P., Davies R. D., Lang R. H., Bates B., 2001, A&A, 380, 683
Smoker J. V., et al., 2003, MNRAS, 346, 119
Smoker J. V., Bagnulo S., Cabanac R., Ledoux C., Jehin E., Melo S., Keenan F. P., 2011, MNRAS, 414, 59
Smoker J. V., Ledoux, C. Jehin E. Keenan F. P., Kennedy M., Cabanac R., Melo, C., 2014, MNRAS, 438, 1127
Smoker J. V., Keenan F. P., Fox A., 2015, 582, 59
Songaila A., 1981, ApJ, 243, L19
Songaila A., Cowie L. L., York D. G., 1981, ApJ, 248, 956
Songaila A., Blades J. C., Hu E. M., Cowie L. L., 1986, ApJ, 303, 198
Stanimirović S., Hoffman S., Heiles C., Douglas K. A., Putman, M., Peek J. E. G., 2008, ApJ, 680, 276
Staveley-Smith L., Kim S., Calabretta M. R., Haynes R. F., Kesteven M., 2003, MNRAS, 339, 87
Thom C., Putman M. E., Gibson B. K., Christlieb N., Flynn C., Beers T. C., Wilhelm R., Lee Y. S., 2006, ApJ, 638, L97
Thom C., Peek J. E. G., Putman M. E., Heiles Carl., Peek K. M. G., Wilhelm R., 2008, ApJ, 684, 364
Vallerga J. V., Vedder P. W., Craig N., Welsh B. Y., 1993, ApJ, 411, 729
van Loon J. Th., Smith K. T., McDonald I., Sarre P. J., Fossey

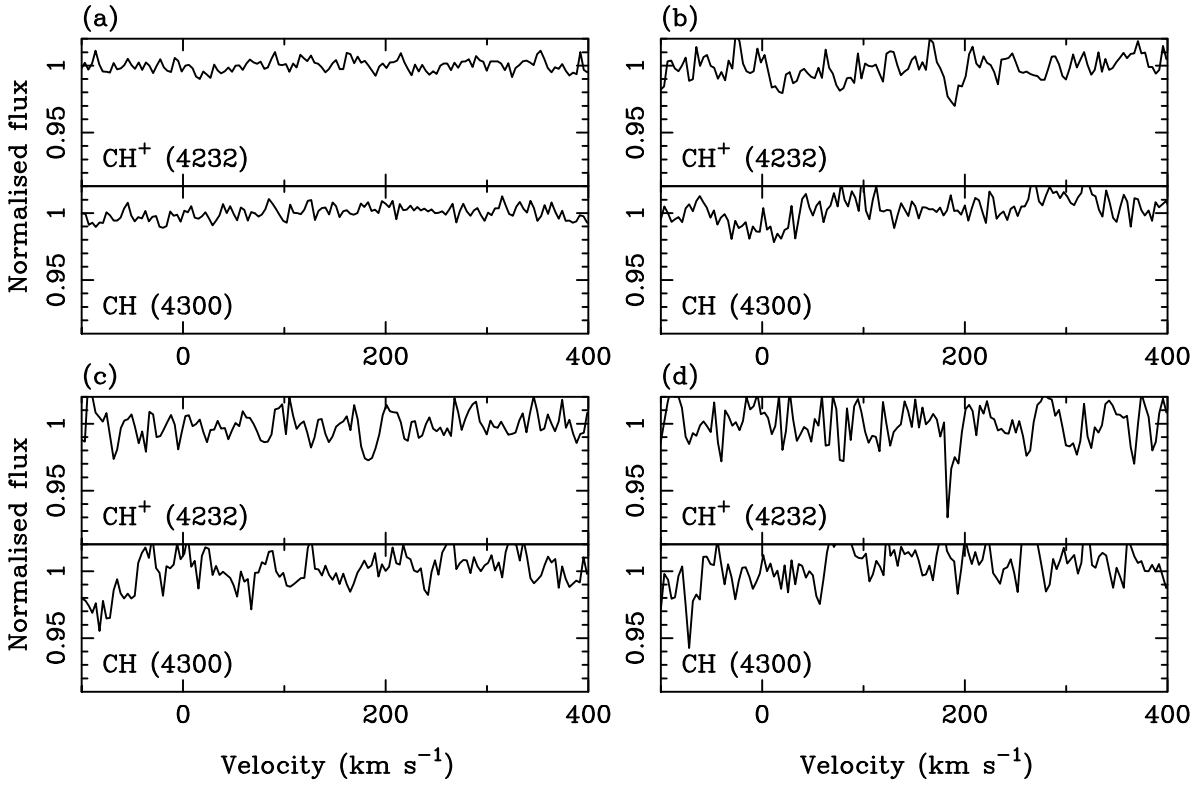

Figure 14. CH^+ (4232Å) and CH (4300Å) profiles towards NGC 2004. Only three sightlines show tentative molecular line absorption at Magellanic Cloud velocities, and none show molecular absorption at Galactic or I/HVC velocities.

S. J., Sharp R. G., 2009, MNRAS, 399, 195
van Loon J. Th., Bailey M., Tatton B. L., et al., 2013, A&A, 550, 108
van Woerden H., Schwarz U. J., Peletier R. F., Wakker B. P., Kalberla P. M. W., 1999, Nat., 400, 138
Wakker B. P., van Woerden H., 1997, ARA&A, 35, 217
Wakker B. P., Mathis J. S., 2000, ApJ, 544, 107
Wakker B. P., 2001, ApJS, 136, 463
Wakker B. P., et al., 2007, ApJ, 670, 113
Wakker B. P., York D. G., Wilhelm R., Barentine J. C., Richter P., Beers T. C., Ivezic Z., Howk J. C., 2008, ApJ, 672, 298
Wallace P., Clayton C., 1996, RV, Starlink User Note SUN 78, Rutherford Appleton Laboratory/CCLRC
Wayte S. R., 1990, ApJ, 355, 473
Wegner et al., 2000, A&AS, 143, 9
Welsh B. Y., Wheatley J., Lallement R., 2009, PASP, 121, 606
Welty D. E., Lauroesch J. T., Blades J. C., Hobbs L. M., York D. G., 1997, ApJ, 489, 672
Welty D. E., Frisch P. C., Sonneborn G., York D. G., 1999, ApJ, 512, 636
Welty D., Fitzpatrick E. L., 2001, ApJ, 551, 175
Welty D. E., Federman S. R., Gredel R., Thorburn J. A., Lambert D. L., 2006, ApJS, 165, 138
Welty D. E., Xue R., Wong T., 2012, ApJ, 745, 173
Westmeier T., Brüns C., Kerp J., 2008, MNRAS, 390, 1691

APPENDIX A: ONLINE MATERIAL

Table A1. FEROS and UVES-observed stars towards the Magellanic Clouds. Stars with RA<2^h are in the SMC and with RA>3^h in the LMC. S/N ratios are per pixel.

Name	Alt name	R.A. (J2000)	Dec. (J2000)	l (deg.)	b (deg.)	m_v (mag)	m_b (mag)	Spect. type	S/N CaK	S/N NaD	Inst.
HV 1328	SMC V0172	00 32 54.90	-73 49 19.1	304.70	-43.24	14.17	14.116	–	–	55	U
HV 1333	SMC V0189	00 36 03.46	-73 55 58.8	304.39	-43.15	15.87	14.702	–	–	35	U
HV 1335	SMC V0193	00 36 55.70	-73 56 27.9	304.31	-43.15	15.399	14.746	–	–	50	U
HV 817	–	00 39 16.55	-72 01 58.4	304.26	-45.06	14.44	13.77	–	–	50	U
HV 1345	SMC V0214	00 40 38.60	-73 13 14.2	304.01	-43.88	15.428	14.779	–	–	15	U
HV 822	–	00 41 55.48	-73 32 23.7	303.86	-43.57	14.39	13.95	–	–	30	U
HV 1365	–	00 42 00.00	-73 44 00.0	303.84	-43.38	15.55	14.94	–	–	30	U
SV* HV 823	–	00 43 48.50	-73 36 50.0	303.67	-43.50	13.99	13.39	–	–	60	U
AzV 014	Sk 9	00 46 32.63	-73 06 05.7	303.43	-44.02	13.59	13.77	O3-4V+neb	60	–	U
AzV 015	Sk 10	00 46 42.14	-73 24 55.7	303.40	-43.71	12.984	13.176	O6.5II(f)	60	–	U
AzV 018	Sk 13	00 47 12.22	-73 06 33.2	303.36	-44.01	12.52	12.48	OB	120	100	U
AzV 022	Sk 15	00 47 38.70	-73 07 48.8	303.31	-44.00	12.15	12.25	B2I	70	–	U
AzV 023	Sk 17	00 47 38.91	-73 22 53.9	303.31	-43.74	12.324	12.236	B2I	120	200	U
SMC 9251	–	00 47 47.60	-73 17 28.0	303.30	-43.83	14.90	14.76	–	70	–	U
AzV 026	Sk 18	00 47 50.04	-73 08 21.0	303.30	-43.99	12.35	12.55	O7III+neb	250	–	U
AzV 047	SMC 11925	00 48 51.48	-73 25 58.5	303.19	-43.69	13.314	13.496	O8III((f))	60	60	U
AzV 065	Sk 33	00 50 06.08	-73 07 45.2	303.07	-44.00	11.12	11.00	B5I	100	200	U
AzV 070	Sk 35	00 50 18.11	-72 38 10.0	303.05	-44.49	10.96	12.40	O9.5Iw	130	130	U
AzV 075	Sk 38	00 50 32.39	-72 52 36.5	303.02	-44.25	12.604	12.756	O5III(f+)	75	–	U
AzV 80	SMC 17457	00 50 43.80	-72 47 41.5	303.01	-44.33	13.24	13.376	O4-6n(f)p	100	80	U
DZ Tuc	SMC 17504	00 50 44.70	-73 16 05.4	303.00	-43.86	15.37	15.44	B0-B0.5V	25	30	U
AzV 95	SMC 19650	00 51 21.65	-72 44 14.4	302.94	-44.39	13.64	13.83	O7III((f))	100	60	U
AzV 104	SMC 20656	00 51 38.43	-72 48 06.1	302.91	-44.33	13.064	13.226	B0.5Ia	70	–	U
LIN 200	Bruck 60 14	00 51 57.74	-73 14 22.0	302.88	-43.89	17.493	17.20	–	10	50	U
AzV 120	SMC 23151	00 52 15.24	-72 09 15.8	302.84	-44.97	14.14	14.43	O9.5III	120	60	U
ESHC 05	–	00 52 06.43	-73 06 29.4	302.86	-44.02	14.2	13.983	–	–	100	U
ESHC 03	–	00 52 21.50	-73 13 33.0	302.84	-43.90	–	–	–	30	25	U
ESHC 02	–	00 52 32.60	-73 17 08.0	302.82	-43.84	16.957	17.012	B2IV-V	20	35	U
ESHC 07	–	00 52 52.60	-73 18 34.0	302.79	-43.82	15.417	15.254	–	120	250	U
ESHC 01	LIN 232	00 53 02.80	-73 17 59.4	302.77	-43.83	15.072	15.079	B4III	20	–	U
ESHC 04	–	00 53 56.75	-73 10 29.4	302.68	-43.95	14.901	15.049	–	40	40	U
OGLE 13487	–	00 54 33.22	-73 10 39.0	302.62	-43.95	15.51	15.69	–	200	–	U
ESHC 06	LIN 264	00 54 37.60	-73 04 56.0	302.61	-44.04	15.128	15.177	–	60	30	U
HV 1645	–	00 55 19.76	-73 14 42.2	302.54	-43.88	20.10	16.84	Mira	–	20	U
LHA 115-S 23	AzV 172	00 55 53.81	-72 08 59.0	302.45	-44.97	13.29	13.25	B8[e]Ib	10	30	F
N330 ROB B18	SMC 35727	00 56 03.70	-72 27 12.8	302.44	-44.67	15.57	15.79	O9.5V	30	–	U
N330 ROB B28	N330 BAL 254	00 56 06.80	-72 28 34.9	302.44	-44.65	15.52	15.71	B0Ve	30	–	U
N330 ROB B32	N330 ELS 36	00 56 10.65	-72 28 10.1	302.43	-44.65	14.74	14.85	B2II	35	–	U
N330 ROB B16	–	00 56 18.56	-72 26 45.4	302.42	-44.68	13.92	13.98	A2II	60	40	U
N330 ROB B13	N330 ELS 125	00 56 20.11	-72 27 02.3	302.41	-44.67	15.58	15.78	B2III/IVe	20	–	U
N330 ROB B38	N330 ELS 121	00 56 22.56	-72 28 35.9	302.41	-44.65	12.474	12.366	A5I	–	70	U
N330 ROB B04	–	00 56 30.90	-72 28 19.0	302.39	-44.65	15.41	15.58	B1.5IVe	25	–	U
AzV 187	Sk 68	00 57 31.73	-71 19 59.3	302.23	-45.79	11.96	12.09	OB	55	85	F
N346 ELS 26	SMC 42719	00 58 14.24	-72 10 45.0	302.20	-44.94	19.15	17.98	B0IV(Nstr)	–	65	U
N346 ELS 12	AzV 202	00 58 14.48	-72 07 29.8	302.19	-44.99	14.18	14.34	B1Ib	–	60	U
N346 ELS 28	–	00 58 17.35	-72 10 50.8	302.19	-44.94	14.73	14.94	OC6Vz	–	70	U
AzV 207	SMC 43724	00 58 33.17	-71 55 47.0	302.15	-45.19	14.13	14.35	O7V	40	60	U
AzV 210	Sk 73	00 58 35.79	-72 16 25.0	302.16	-44.84	12.63	12.66	OB	50	–	U
N346 ELS 18	N346 ELS 18	00 58 47.03	-72 13 01.6	302.14	-44.90	14.66	14.78	O9.5IIIe	–	40	U
AzV 214	SMC 44784	00 58 54.76	-72 13 17.2	302.13	-44.90	13.40	13.39	B1Ia	100	90	U
AzV 215	Sk 76	00 58 55.62	-72 32 08.5	302.14	-44.58	12.65	12.75	OB	60	–	U
N346 ELS 07	SMC 44908	00 58 57.40	-72 10 33.5	302.12	-44.94	13.82	14.13	O4V((f))	–	110	U
AzV 216	–	00 58 59.13	-72 44 34.0	302.15	-44.37	14.15	14.32	B1-3II:	40	–	U
N346 MPG 355	SMC 45068	00 59 00.75	-72 10 28.2	302.11	-44.94	12.61	12.80	O2III(f)	–	100	U
N346 MPG 368	–	00 59 01.80	-72 10 31.2	302.11	-44.94	13.95	14.18	O6:V	–	120	U
N346 MPG 487	–	00 59 06.71	-72 10 41.3	302.10	-44.94	14.19	14.33	O8V	–	70	U

Table A1. continued.

Name	Alt name	R.A. (J2000)	Dec. (J2000)	l (deg.)	b (deg.)	m_v (mag)	m_b (mag)	Spect. type	S/N CaK	S/N NaD	Inst.
N346 ELS 51	SMC 45459	00 59 08.68	-72 10 14.1	302.10	-44.95	15.17	15.40	O7Vz	–	30	U
N346 ELS 33	N346 SSN 37	00 59 11.64	-72 09 57.6	302.09	-44.95	14.82	15.07	O8V	–	30	U
N346 ELS 22	SMC 45935	00 59 18.58	-72 11 10.1	302.08	-44.93	14.65	14.91	O9V	–	40	U
N346 ELS 10	AzV 226	00 59 20.73	-72 17 10.7	302.08	-44.83	14.12	14.19	O7IIIn((f))	–	80	U
HD 5980	AzV 229	00 59 26.57	-72 09 53.9	302.07	-44.95	11.13	11.31	WN3+OB	–	60	U
N346 ELS 46	–	00 59 31.88	-72 13 35.2	302.06	-44.89	15.16	15.44	O7Vn	–	40	U
AzV 232	Sk 80	00 59 31.96	-72 10 46.3	302.06	-44.93	12.12	12.31	O7Iaf+	120	150	U
AzV 235	Sk 82	00 59 45.75	-72 44 56.5	302.07	-44.37	12.02	12.20	B0Iaw	100	–	U
N346 ELS 31	SMC 47478	00 59 54.08	-72 04 31.0	302.01	-45.04	14.81	15.05	O8Vz	–	60	U
AzV 243	Sk 84	01 00 06.71	-72 47 19.0	302.03	-44.32	13.71	13.91	O6V	80	–	U
AzV 242	Sk 85	01 00 06.86	-72 13 57.5	301.10	-44.88	11.7	11.5	B0.7Iaw	250	200	U
AzV 304	SMC 53474	01 02 21.47	-72 39 14.7	301.79	-44.45	14.66	14.77	B0.5V	70	–	U
AzV 321	SMC 54958	01 02 57.07	-72 08 09.1	301.68	-44.96	13.66	13.82	O9Ib	110	70	U
AzV 372	Sk 116	01 04 55.74	-72 46 48.1	301.54	-44.31	12.494	12.646	O9.5Iabw	90	–	U
AzV 388	SMC 62400	01 05 39.52	-72 29 27.1	301.43	-44.60	13.86	14.12	O4V	50	–	U
AzV 398	SMC 63413	01 06 09.81	-71 56 00.8	301.31	-45.15	13.94	13.98	O9Ia:	80	65	U
MA93 1589	–	01 06 28.85	-71 52 04.9	301.27	-45.21	15.411	15.135	A5	100	–	U
AzV 404	Sk 128	01 06 29.27	-72 22 08.4	301.33	-44.71	11.7	11.8	OB	200	120	U
LHA 115-S 52	HD 6884	01 07 18.22	-72 28 03.7	301.25	-44.61	10.32	10.23	B9Iae	45	125	F
AzV 440	SMC 68756	01 08 56.01	-71 52 46.8	301.00	-45.18	14.44	14.58	O7V	60	35	U
AzV 456	Sk 143	01 10 55.77	-72 42 56.3	300.91	-44.34	12.98	12.89	OB	70	200	U
AzV 462	Sk 145	01 11 25.92	-72 31 20.9	300.83	-44.52	12.464	12.596	OB	30	65	F
AzV 469	Sk 148	01 12 29.00	-72 29 29.1	300.71	-44.55	13.014	13.176	O8II	100	–	U
HV 2195	–	01 14 28.05	-72 39 53.5	300.54	-44.36	12.99	12.51	F5Ib	–	50	U
AzV 488	Sk 159	01 15 08.88	-73 21 24.3	300.51	-43.66	11.77	11.90	B0.5Iaw	130	130	U
AzV 483	Sk 156	01 15 28.63	-73 19 50.1	300.55	-43.69	11.85	11.93	OB	50	70	F
SK 160	AzV 190	01 17 05.15	-73 26 36.0	300.41	-43.56	13.12	13.30	OB:	120	150	U
SK 190	–	01 31 27.96	-73 22 14.3	299.00	-43.45	13.37	13.59	O7.5(f)np	90	65	U
SK-67 2	RMC 51	04 47 04.45	-67 06 53.1	278.36	-36.79	11.219	11.26	B1.5Ia	50	130	F
SK -67 05	RMC 53	04 50 18.92	-67 39 38.1	278.89	-36.32	11.2	11.377	O9.7Ib	220	–	U
SK-66 1	RMC 56	04 52 19.09	-66 43 53.3	277.72	-36.41	11.603	11.635	B2Ia	30	60	F
SK-66 5	RMC 57	04 53 30.03	-66 55 28.3	277.90	-36.24	10.68	10.76	B3Iab	30	130	F
SK-67 14	Sk -67 14	04 54 31.89	-67 15 24.7	278.27	-36.05	11.376	11.541	B1.5Ia	40	80	F
SK -66 18	–	04 55 59.80	-65 58 29.8	276.69	-36.25	13.294	13.467	O6V((f))	100	80	U
SK -69 43	HD 268809	04 56 10.46	-69 15 38.2	280.58	-35.33	11.866	11.964	OB	30	70	F
LH 10-3061	–	04 56 42.46	-66 25 18.1	277.20	-36.07	13.595	13.491	ON2III(f*)	90	75	U
SK -66 35	HD 268732	04 57 04.47	-66 34 38.5	277.38	-35.99	11.494	11.587	OB	50	80	F
SK -69 50	LMC 33053	04 57 15.09	-69 20 19.9	280.64	-35.22	13.204	13.366	O7(f)(n)p	100	80	U
SK -67 22	Brey 10a	04 57 27.44	-67 39 02.9	278.64	-35.67	13.314	13.496	Of	110	–	U
LHA 120-S 12	SK -67 23	04 57 36.80	-67 47 37.5	278.80	-35.62	12.66	12.526	B0.5Ie	35	70	F
SK -69 52	HD 268867	04 57 48.90	-69 52 22.3	281.24	-35.02	11.392	11.399	OB	50	–	U
SK -67 28	GV 135	04 58 39.24	-67 11 18.7	278.05	-35.69	12.082	12.269	B0.7Ia	35	85	F
SK -68 26	GV 167	05 01 32.24	-68 10 42.9	279.14	-35.17	11.728	11.85	BC2Ia	35	70	F
LHA 120-S 155	RMC 71	05 02 07.39	-71 20 13.1	282.82	-34.25	10.60	10.55	OB	35	70	F
SK -69 59	HD 268960	05 03 12.70	-69 01 37.0	280.09	-34.80	12.01	12.166	B0Ia	25	45	F
SK -67 38	LMC 59721	05 03 29.73	-67 52 25.1	278.72	-35.07	13.494	13.716	OB	100	80	U
SK -70 50	HD 269009	05 03 45.85	-70 11 57.5	281.45	-34.44	11.0	11.1	OB	50	105	F
SK -70 60	LMC 64006	05 04 40.78	-70 15 34.6	281.49	-34.35	13.646	13.914	O4-O5V:n	110	–	U
SK -68 39	–	05 04 50.17	-68 07 52.4	278.99	-34.88	11.988	12.039	B2.5Ia	50	115	F
SK -70 69	LMC 65981	05 05 18.70	-70 25 49.8	281.68	-34.25	13.616	13.854	O3V(f)	75	50	U
SK -68 41	GV 195	05 05 27.11	-68 10 02.6	279.02	-34.82	11.868	12.01	B0.5Ia	40	100	F
SK -68 45	–	05 06 07.28	-68 07 06.2	278.94	-34.77	11.92	12.007	OB	30	70	F
SK -70 78	HD 269074	05 06 16.04	-70 29 35.7	281.72	-34.16	11.0	11.1	OB	50	70	F
SK -68 52	HD 269050	05 07 20.41	-68 32 08.6	279.40	-34.56	11.581	11.54	B0Ia	50	–	U
OGLE J050724	–	05 07 24.62	-68 29 32.7	279.35	-34.56	–	16.76	Ecl. Bin	45	–	U
SK -68 63	HIP 24080	05 10 22.79	-68 46 23.8	279.60	-34.23	10.52	10.52	B1.5eq	200	–	U

Table A1. continued.

Name	Alt name	R.A. (J2000)	Dec. (J2000)	l (deg.)	b (deg.)	m_v (mag)	m_b (mag)	Spect. type	S/N CaK	S/N NaD	Inst.
BI 108	LMC 94226	05 13 43.05	-69 18 36.9	280.15	-33.82	13.222	13.332	B1:II:	130	–	U
SK -69 83	HD 269244	05 14 29.64	-69 29 43.4	280.35	-33.72	11.435	11.612	OB	30	70	F
LHA 120-S 93	GV 566	05 16 31.80	-68 22 09.1	278.98	-33.77	12.81	12.69	A0:I:	25	45	F
SK -69 89	HD 269311	05 17 17.57	-69 46 44.2	280.62	-33.42	11.999	11.428	OB	40	80	F
LHA 120-S 96	SK -69 94	05 18 14.35	-69 15 01.1	279.98	-33.44	9.635	9.565	A5Iaeq	50	165	F
BI 128	–	05 18 19.77	-65 49 14.6	275.92	-34.06	13.447	13.745	O...	80	40	U
SK -67 78	HD 269371	05 20 19.08	-67 18 05.7	277.64	-33.62	11.3	11.0	OB	30	95	F
LHA 120-S 30	SK -68 73	05 22 59.73	-68 01 46.3	278.45	-33.24	11.71	11.46	Bep	35	95	F
SK -67 90	HD 269440	05 23 00.66	-67 11 22.1	277.46	-33.38	11.282	11.378	B1Ia	55	120	F
SK -67 112	HD 269545	05 26 56.48	-67 39 35.0	277.94	-32.93	11.77	11.90	OB	30	80	F
SK -66 100	–	05 27 45.47	-66 55 15.2	277.06	-32.96	12.976	13.204	O6II(f)	110	70	U
SK -68 92	GV 315	05 28 16.17	-68 51 45.6	279.33	-32.63	11.64	11.71	OB	45	80	F
HD 269599	RMC 105	05 28 22.73	-69 08 31.7	279.66	-32.60	10.24	10.03	–	35	30	F
SK -66 106	–	05 29 00.99	-66 38 27.8	276.71	-32.87	12.64	12.72	OB	55	120	F
LHA 120-S 116	RMC 110	05 30 51.48	-69 02 58.6	279.51	-32.37	10.52	10.28	F0Iae	30	70	F
SK -66 118	GV 341	05 30 51.91	-66 54 09.1	276.99	-32.66	11.674	11.776	OB	45	55	F
SK -67 150	–	05 30 01.71	-67 00 53.4	277.13	-32.68	12.034	12.24	OB	50	110	F
SK -71 42	HD 269660	05 30 47.78	-71 04 02.3	281.87	-32.06	11.15	11.19	B1Ia	55	95	F
SK -68 111	HD 269668	05 31 00.84	-68 53 57.1	279.33	-32.38	10.161	12.01	OB	45	75	F
SK -67 169	–	05 31 51.59	-67 02 22.3	277.14	-32.55	12.06	12.18	B1Ia	45	90	F
HDE 269702	SK -67 168	05 31 52.12	-67 34 20.8	277.76	-32.48	11.69	11.99	O8I(f)p	125	70	U
SK -68 114	HD 269700	05 31 52.28	-68 32 38.9	278.90	-32.35	10.56	10.54	BN?2Ia+	25	45	F
SK -67 172	HD 269713	05 32 07.32	-67 29 14.0	277.66	-32.47	11.81	11.88	OB	30	70	F
SK -67 173	LH 76-51	05 32 10.75	-67 40 25.0	277.88	-32.44	11.92	12.04	OB	30	45	F
SK -67 199	HD 269777	05 34 18.45	-67 18 13.7	277.41	-32.28	11.05	11.06	B3Ia	40	80	F
SK -67 206	–	05 34 55.11	-67 02 37.5	277.10	-32.25	9.862	12.00	OB	45	80	F
BI 237	LMC 164942	05 36 14.63	-67 39 19.2	277.80	-32.06	13.790	13.830	O2V(f*)	90	60	U
SK -69 214	CPD-69 419	05 36 16.42	-69 31 27.0	279.99	-31.83	12.279	12.19	B0.7Ia	30	70	F
HD 37974	SK -69 216	05 36 25.87	-69 22 55.9	279.82	-31.84	11.10	10.959	Be	25	90	F
SK -66 171	HD 269889	05 37 02.42	-66 38 36.9	276.61	-32.08	10.246	12.19	OB	95	50	U
SK -69 228	CPD-69 436	05 37 09.18	-69 20 19.5	279.76	-31.78	12.19	12.12	BC1.5Ia	40	105	F
BI 253	LMC 168644	05 37 34.46	-69 01 10.2	279.38	-31.78	13.56	13.70	O2V(f*)	105	90	U
SK -69 237	SK -69 237	05 38 01.31	-69 22 14.1	279.79	-31.70	12.05	12.08	B1Ia	30	90	F
LHA 120-S 134	HD 38489	05 40 13.33	-69 22 46.5	279.79	-31.70	12.296	12.215	B[e]	30	70	F
SK-69 270	HD 269997	05 41 21.19	-69 04 38.6	279.41	-31.44	11.36	11.20	B2.5Ia	40	110	F
SK-69 274	HD 269992	05 41 27.68	-69 48 03.7	280.25	-31.35	11.27	11.22	B2.5Ia	45	120	F
SK-70 111	HD 269993	05 41 36.79	-70 00 52.6	280.50	-31.32	11.78	11.516	OB	35	80	F
LHA 120-S 137	–	05 41 48.00	-69 37 00.0	280.03	-31.34	14.198	14.107	BIaePCyg	5	15	F
SK-69 289	CPD-69 514	05 42 49.22	-69 32 52.2	279.94	-31.26	11.4	11.3	OB	35	65	F
SK-67 256	CPD-67 500	05 44 25.02	-67 13 49.6	277.22	-31.32	11.76	11.751	OB	20	85	F
SK-68 171	HD 270220	05 50 22.99	-68 11 24.7	278.30	-30.69	11.960	12.001	B1Ia	20	55	F
SK-70 120	HD 270196	05 51 20.78	-70 17 09.3	280.72	-30.47	11.490	11.6	B1Ia	35	60	F

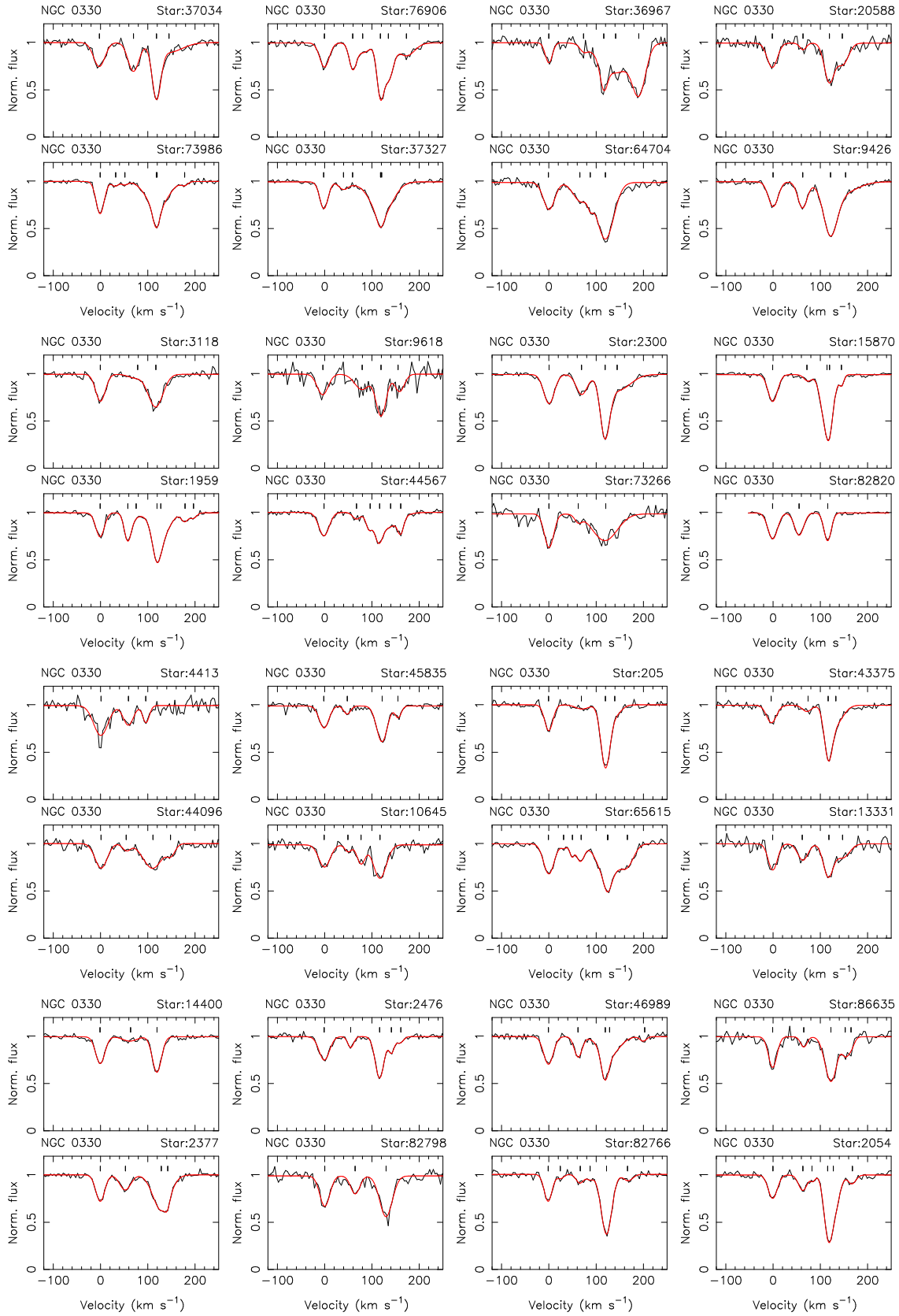

Figure A1. FLAMES-GIRAFFE Ca II K spectra towards NGC 330 showing the spectra of 16 star-to-star pairs in which the maximum difference in the equivalent width was detected between a velocity of +45 and +85 km s^{-1} in the LSR. Each star is only plotted once.

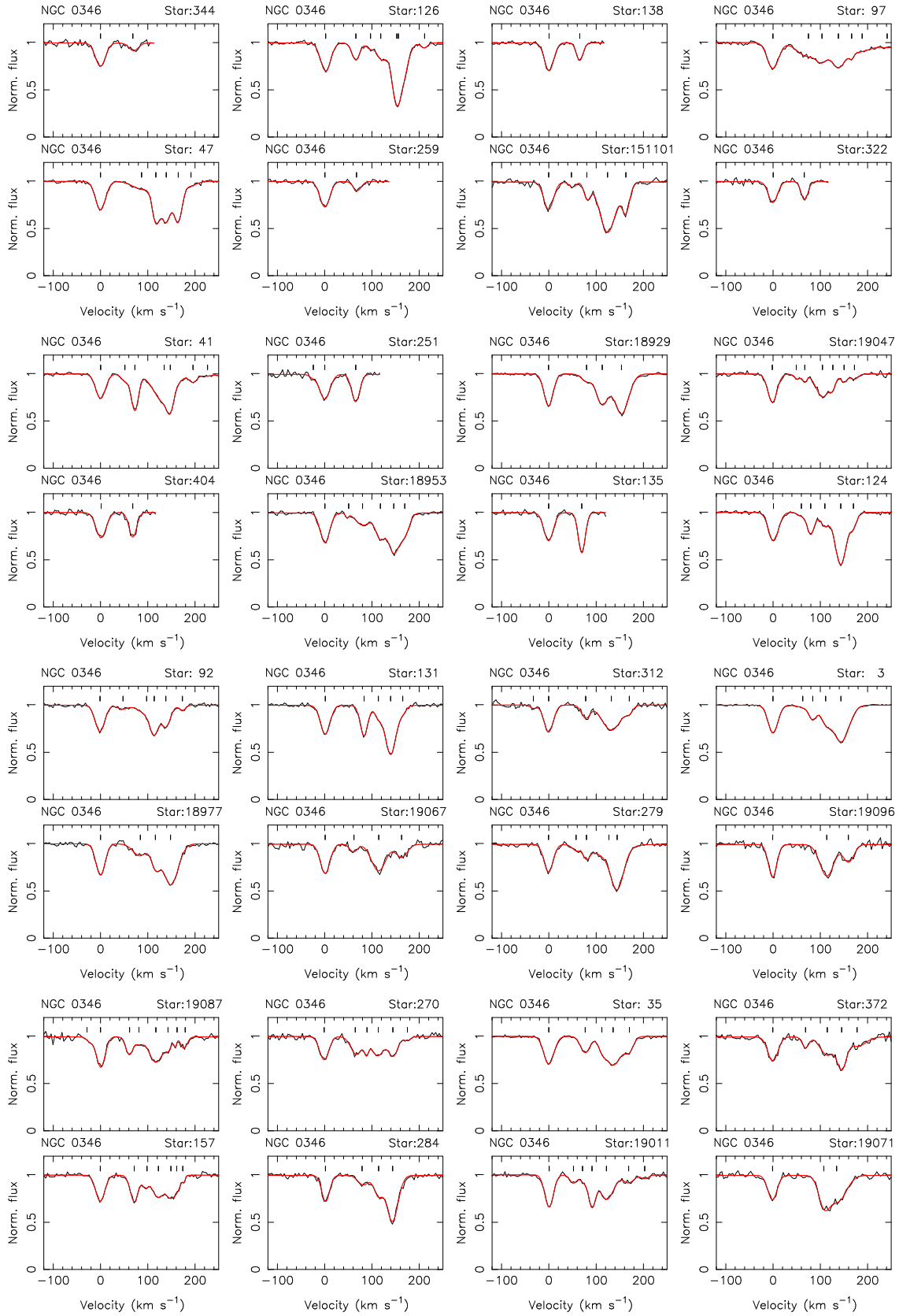

Figure A2. FLAMES-GIRAFFE Ca II K spectra towards NGC 346 showing the spectra of 16 star-to-star pairs in which the maximum difference in the equivalent width was detected between a velocity of +60 and +250 km s^{-1} in the LSR. Each star is only plotted once.

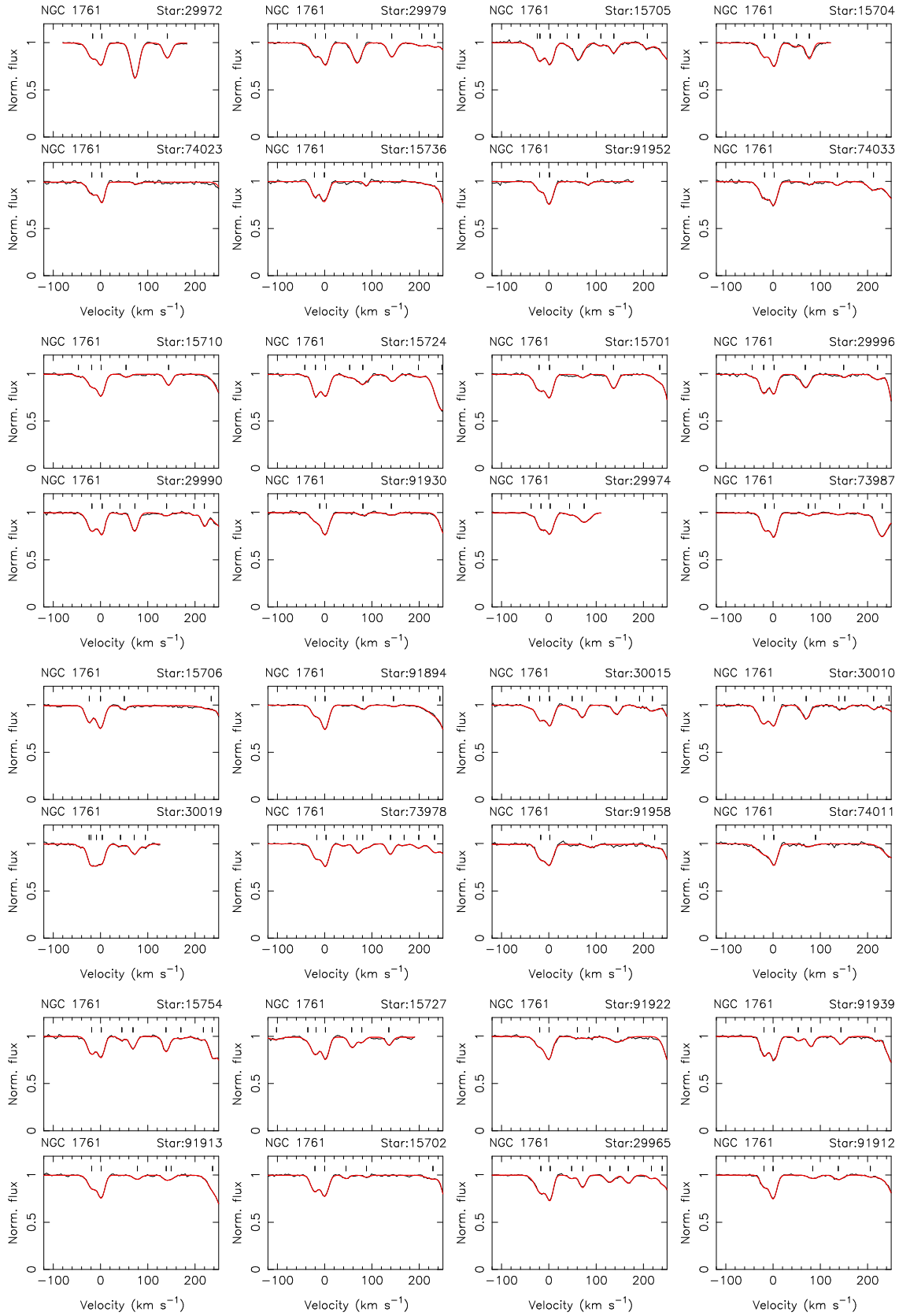

Figure A3. FLAMES-GIRAFFE Ca II K spectra towards NGC 1761 showing the spectra of 16 star-to-star pairs in which the maximum difference in the equivalent width was detected between a velocity of +30 and +105 km s^{-1} in the LSR. Each star is only plotted once.

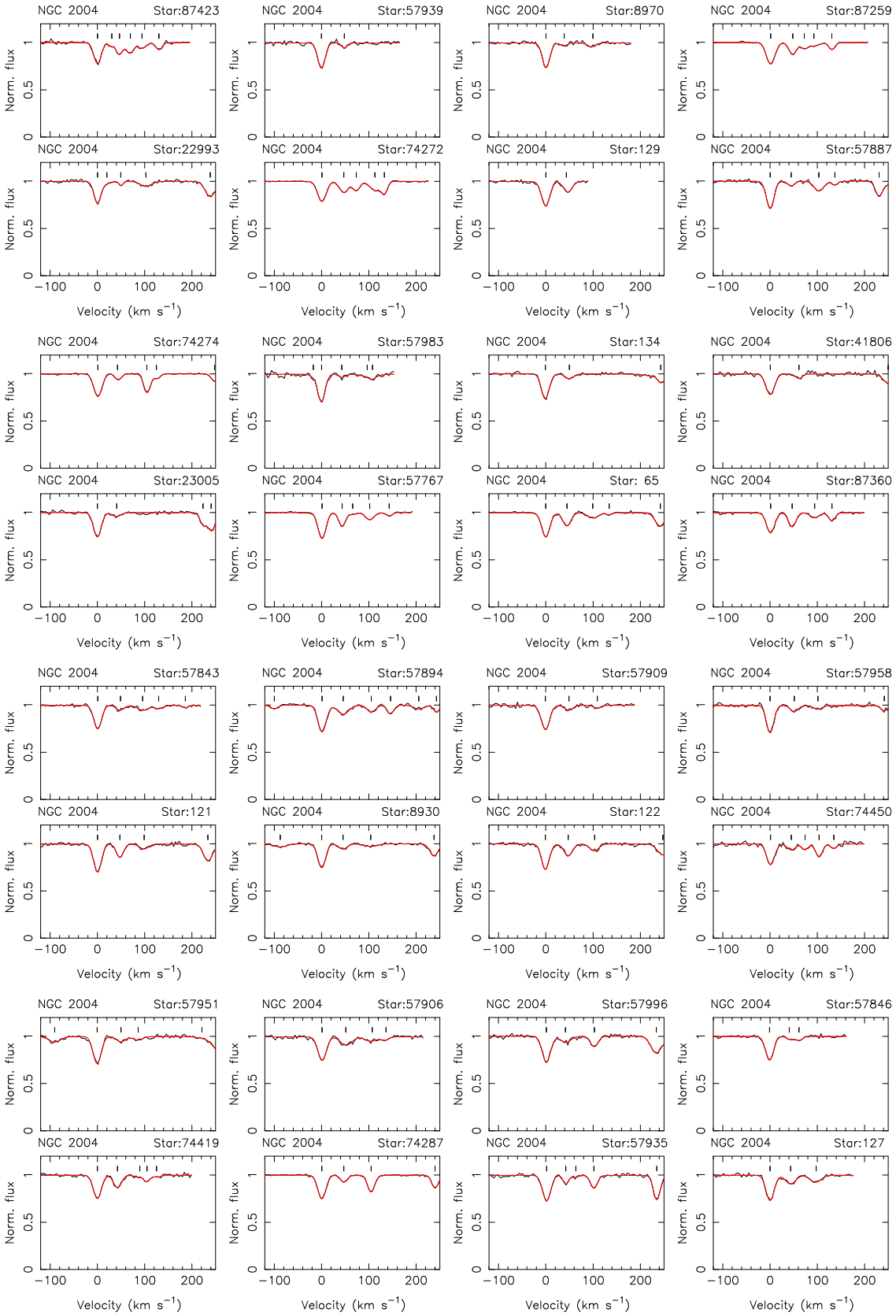

Figure A4. FLAMES-GIRAFFE Ca II K spectra towards NGC 2004 showing the spectra of 16 star-to-star pairs in which the maximum difference in the equivalent width was detected between a velocity of +30 and +75 km s^{-1} in the LSR. Each star is only plotted once.

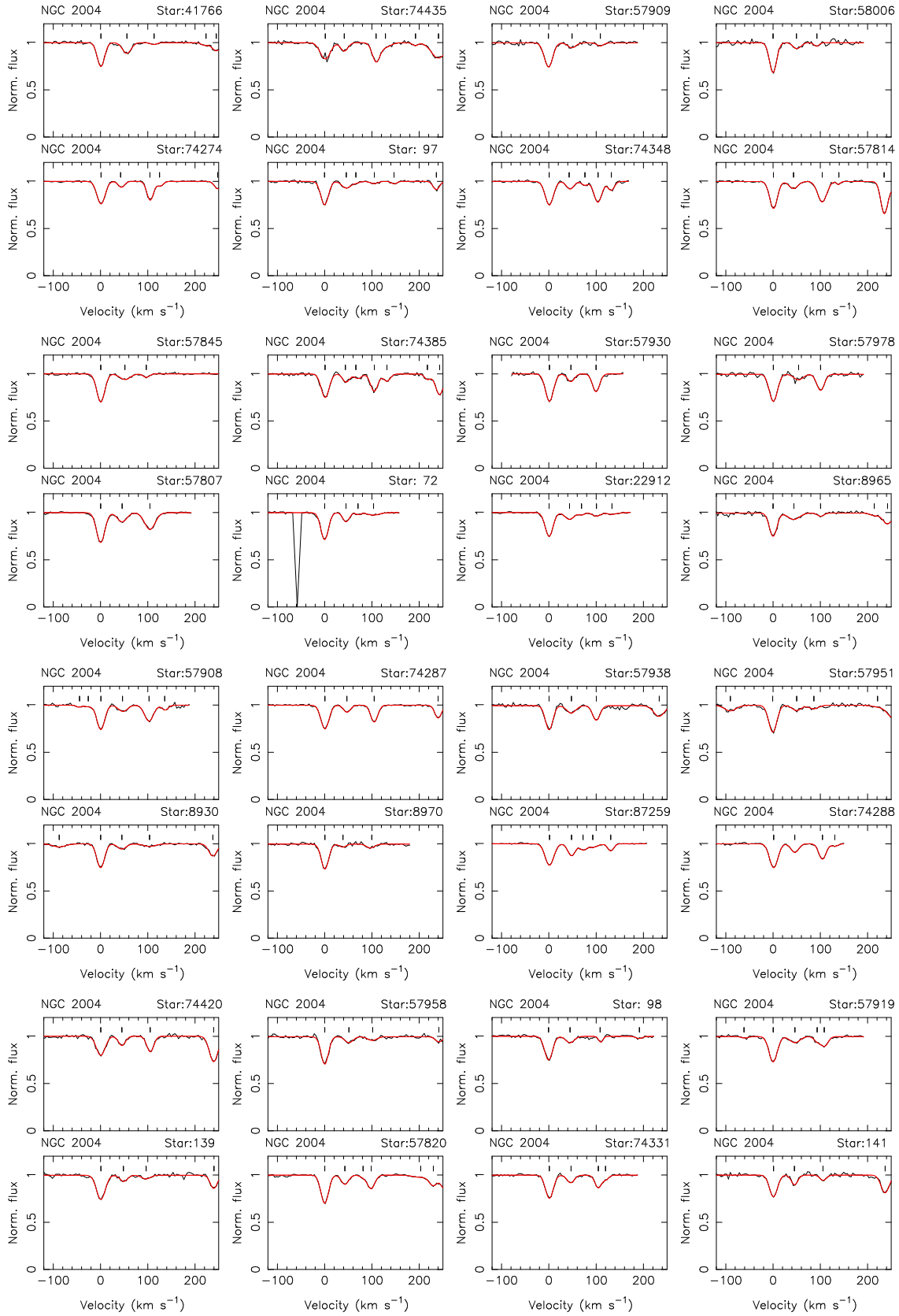

Figure A5. FLAMES-GIRAFFE Ca II K spectra towards NGC 2004 showing the spectra of 16 star-to-star pairs in which the maximum difference in the equivalent width was detected between a velocity of +75 and +130 km s^{-1} in the LSR. Each star is only plotted once.

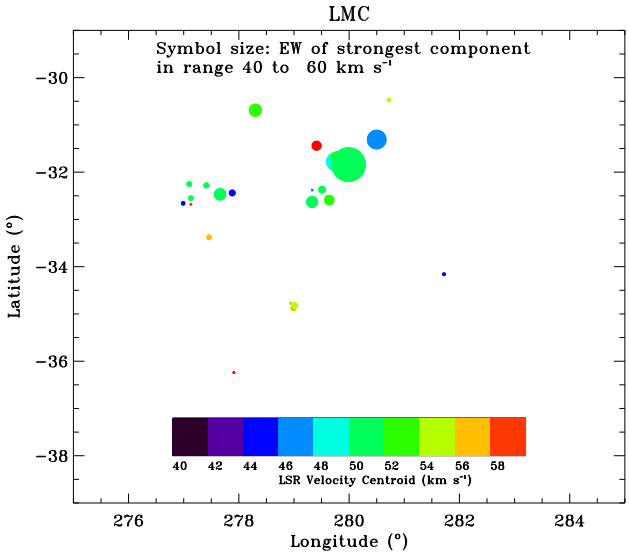

Figure A6. Variation in the Ca II equivalent width for I/HVC components observed with FEROS towards the LMC for velocities between +40 and +60 km s^{-1}.

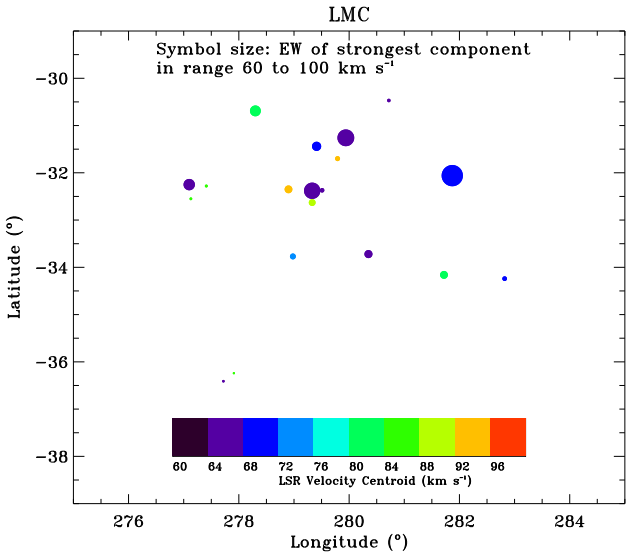

Figure A7. Variation in the Ca II equivalent width for I/HVC components observed with FEROS towards the LMC for velocities between +60 and +100 km s^{-1}.

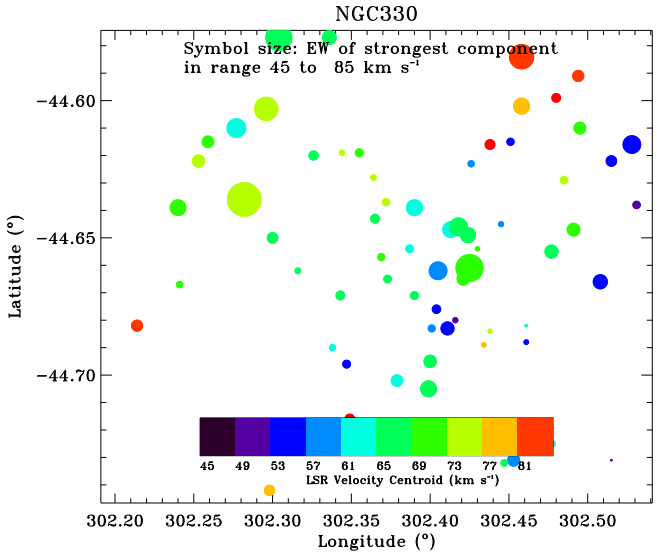

Figure A8. NGC 330 equivalent width and peak velocity between +45 and +85 km s^{-1}.

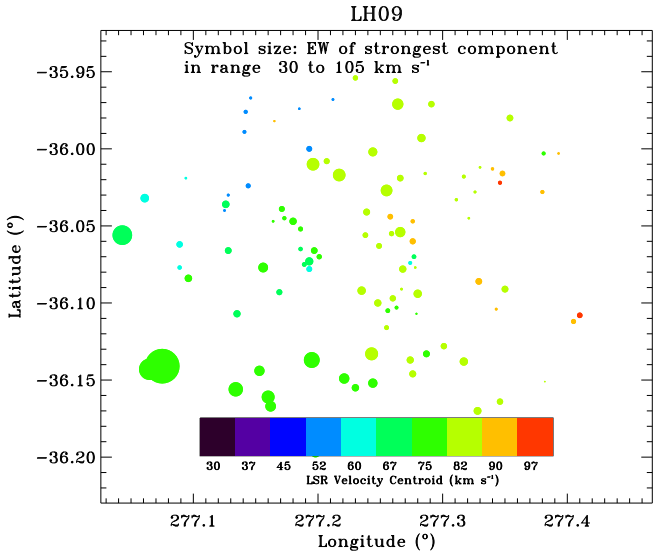

Figure A9. NGC 1761 equivalent width and peak velocity between +30 and +105 km s^{-1}.

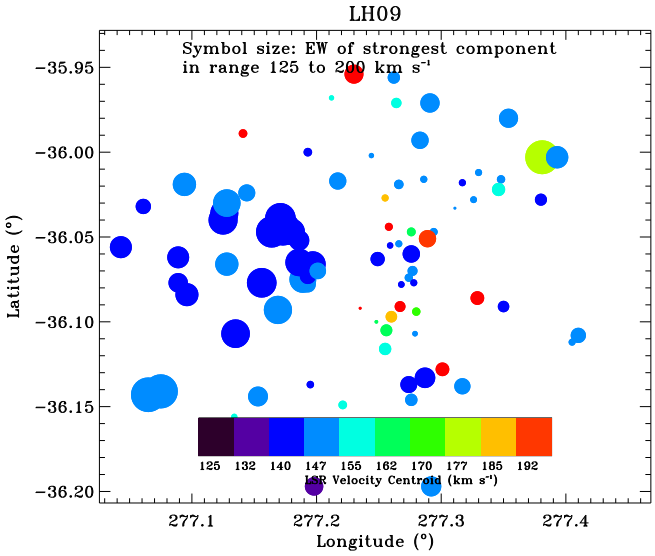

Figure A10. NGC 1761 equivalent width and peak velocity between +125 and +200 km s^{-1}.

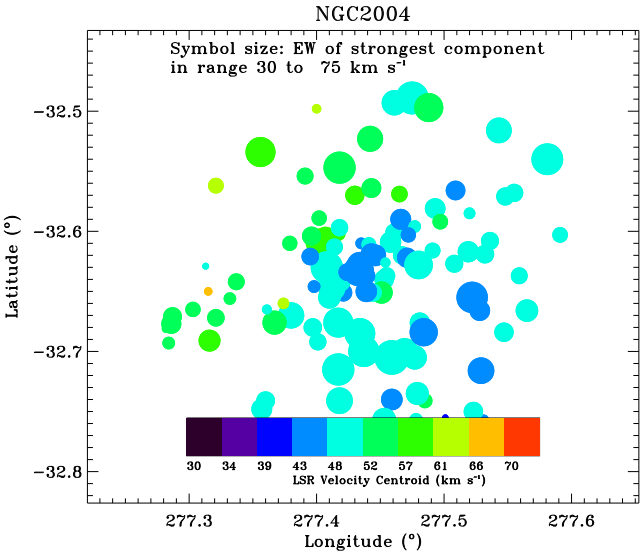

Figure A11. NGC 2004 equivalent width and peak velocity between +30 and +75 km s^{-1}.

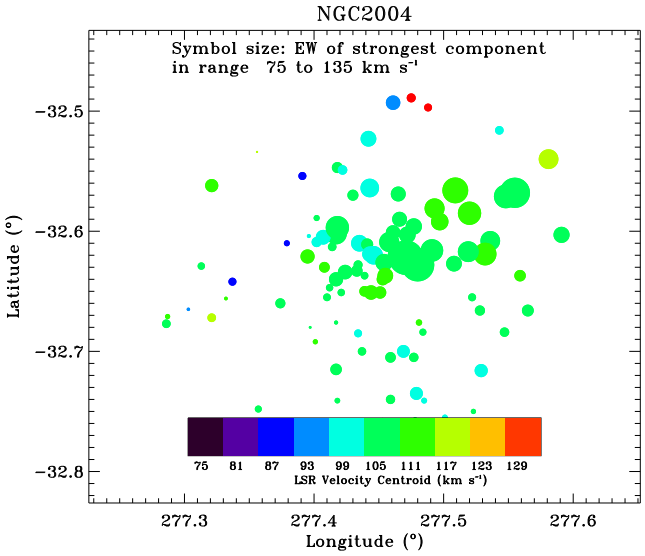

Figure A12. NGC 2004 equivalent width and peak velocity between +75 and +130 km s^{-1}.

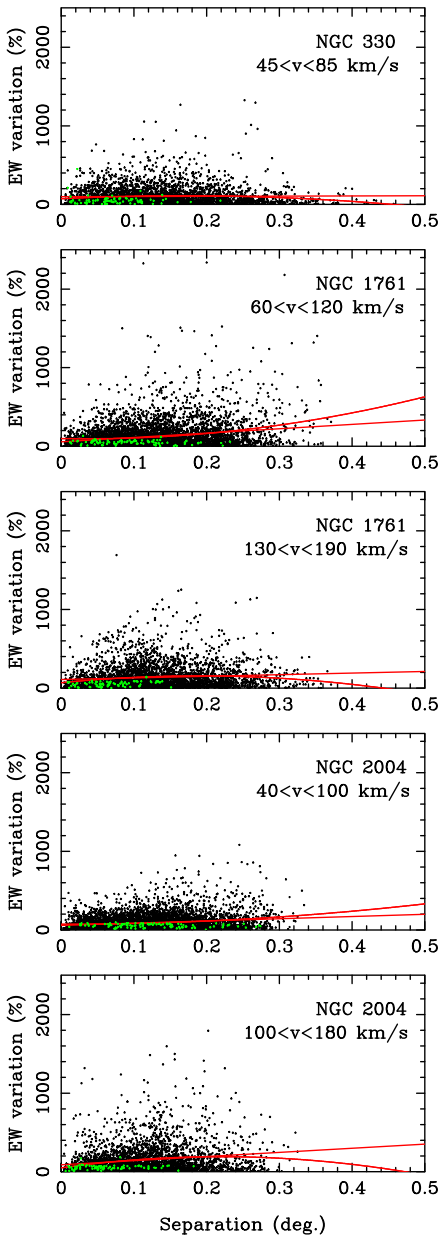

Figure A13. Percentage equivalent width variation in Ca II (100.0×(EW1/EW2)-100.0) plotted against star to star distance in degrees. (a) NGC 330: IVC from +45.0 to +85.0 km s^{-1} (b) NGC 1761: I/HVC from +60.0 to +120.0 km (c) NGC 1761: HVC from +130.0 to +190.0 km/s (d) NGC 2004: I/HVC from +40.0 to +100.0 km/s (e) NGC 2004: I/HVC from +100.0 to +180.0 km/s.